

Aus der Universitätsklinik für Kinder- und Jugendmedizin  
Tübingen  
Abteilung Kinderheilkunde III mit Poliklinik  
(Schwerpunkt: Neuropädiatrie, Entwicklungsneurologie,  
Sozialpädiatrie)

**Brain morphometry in  
Pontocerebellar  
Hypoplasia type 2A**

Inaugural-Dissertation  
zur Erlangung des Doktorgrades  
der Medizin

der Medizinischen Fakultät  
der Eberhard Karls Universität  
zu Tübingen

vorgelegt von  
Ekert, Ephraim Kaspar Anton Heinrich  
2018

**Dekan:** Professor Dr. I. B. Authenrieth  
**1. Berichterstatter:** Professor Dr. I. Krägeloh-Mann  
**2. Berichterstatter:** Professor Dr. U. Ernemann  
**Tag der Disputation:** 19.09.2018

Table of Contents

<b>List of abbreviations</b> .....	<b>5</b>
<b>1. Introduction</b> .....	<b>6</b>
1.1 Overview of Pontocerebellar hypoplasia (PCH) .....	6
1.1.1 Classification of PCH .....	6
1.2 Presentation of Pontocerebellar hypoplasia type 2 .....	6
1.3 Brain development in PCH2A .....	9
1.3.1 Neurological presentation in PCH2A .....	9
1.3.2 Neuropathological findings in PCH2A .....	9
1.4 Genetic testing .....	10
1.5 Magnetic resonance imaging (MRI) in PCH type 2 .....	11
1.5.1 A non-invasive imaging tool: MRI .....	11
1.5.2 MRI findings specific to PCH type 2.....	11
1.6 Aims and Hypothesis .....	12
<b>2. Method</b> .....	<b>14</b>
2.1 Patients.....	14
2.2 MRI data .....	14
2.2.1 Patient MR images .....	14
2.2.2 Longitudinal analysis in five patients .....	16
2.2.3 MRI data of healthy controls .....	16
2.2.4 Analysis of digital MR images .....	18
2.2.5 MRI film processing .....	20
2.2.6 Anatomical definition of brain areas.....	21
2.3 Statistical evaluation .....	22
2.4 Validation method .....	22
2.4.1 Comparison of pixel to voxel-based method .....	22
2.4.2 Intra-class correlation coefficient .....	23
2.4.3 Spatial overlap Index: Dice similarity coefficient .....	23
<b>3. Results</b> .....	<b>25</b>
3.1 Volumetric results.....	25
3.2 Cerebellar volume.....	26
3.2.1 Brain stem volume .....	27
3.2.2 Pons area .....	28
3.2.3 Supratentorial volume .....	29
3.2.4 Frontal lobe volume .....	30
3.2.5 Ratio of Frontal to Supratentorial brain volume .....	31

3.3	Longitudinal analysis .....	32
3.3.1	Cerebellar volume .....	32
3.3.2	Brain stem volume .....	33
3.3.3	Pons area .....	34
3.3.4	Supratentorial volume .....	35
3.3.5	Frontal lobe volume .....	36
3.3.6	Exemplary development of PCH 2A in two patients .....	36
3.4	Validation results .....	39
3.4.1	Pixel contrasted by voxel processing .....	39
3.4.2	Intra-rater variability .....	39
3.4.3	Inter-rater variability .....	39
<b>4.</b>	<b>Discussion .....</b>	<b>40</b>
4.1	Main results .....	40
4.2	Context of findings .....	41
4.3	Hypoplastic vs. atrophic brain development in PCH2 and the hypotheses of this study 43	
4.3.1	Disruption of cerebellar projections.....	43
4.3.2	Progressive neurodegeneration .....	44
4.3.3	Other pathomechanisms .....	45
4.3.4	Significance of disrupted projections.....	45
4.4	Implications of study .....	45
4.5	Methodological aspects .....	46
<b>5.</b>	<b>Abstract.....</b>	<b>48</b>
<b>6.</b>	<b>Zusammenfassung in deutscher Sprache .....</b>	<b>50</b>
<b>7.</b>	<b>Appendix.....</b>	<b>52</b>
<b>8.</b>	<b>Bibliography .....</b>	<b>58</b>
<b>9.</b>	<b>Contributions .....</b>	<b>63</b>
<b>10.</b>	<b>Publications .....</b>	<b>65</b>
<b>11.</b>	<b>Acknowledgements .....</b>	<b>66</b>

## List of abbreviations

95%CI	95% confidence interval
CSF	Cerebral spinal fluid
DICOM	Digital Imaging and Communications in Medicine
DSC	Dice similarity coefficient
FLAIR	Fluid Attenuated Inversion Recovery
ICC	Intra-class Correlation Coefficient
ImageJ	Image Processing and Analysis in Java
IR	Inversion recovery
JPEG	Joint Photographic Experts Group
MRI	Magnetic resonance imaging
NIfTI	Neuroimaging Informatics Technology Initiative
NIH	National Institute of Health
PCH	Pontocerebellar hypoplasia
SEPSECS	O-phosphoseryl-tRNA Selenocystein tRNA synthase
TSEN	tRNA-splicing endonuclease

# 1. Introduction

## 1.1 Overview of Pontocerebellar hypoplasia (PCH)

Pontocerebellar hypoplasia (PCH) is a heterogeneous group of early-onset neurodevelopmental diseases affecting the cerebellum and ventral pons. As more recent research revealed, all share a common pathomechanism involving several genes for RNA processing (Budde et al., 2008; Namavar et al., 2011b). The incidence rate is suggested to be below 1:200 000 with ninety percent of children showing PCH type 2 subtype (Budde et al., 2008; Namavar et al., 2011b, 2011a).

### 1.1.1 Classification of PCH

After an initial description by Brun, R., 1917, there were reports on single cases over the following decades of developmental defects associated with (ponto)cerebellar hypoplasia (Biemond, 1955; Goutières et al., 1977). In 1990, then, Barth et al., proposed the first systematic classification, which they successively modified (Barth, 1993; Barth et al., 1995). A milestone was reached, when the underlying pathomechanism in the form of a *TSEN* mutation was identified (Budde et al., 2008). To date, seven types of pontocerebellar hypoplasia have been described. In all types, except for PCH7 (Anderson et al., 2011), a pathogenic variant has been identified, which relates to RNA processing (Budde et al., 2008; Namavar et al., 2011b, 2016), thus, PCH subtypes, can be described according to their phenotype and genetic mutation.

## 1.2 Presentation of Pontocerebellar hypoplasia type 2

Pontocerebellar hypoplasia type 2 is further categorised into 4 subgroups according to the deficient variant in the transfer RNA splicing endonuclease *TSEN* (compromised of four subunits) and SEPCSECS complexes respectively (Namavar et al., 2011b):

PCH2A (*TSEN54*)

PCH2B (*TSEN2*)

PCH2C (*TSEN34*)

PCH2D (SEPCSECS)

In correlating genotype to phenotype, Budde et al., 2008, and Namavar et al., 2011b showed that ninety percent of PCH2 patients carry a missense mutation (p.A307S) in the TSEN54 gene on chromosome 17.

Abnormal gene products may result in malfunctioning enzyme complexes, which in turn produce deficient proteins (Budde et al., 2008; Namavar et al., 2016). As nonsense mutations in the TSEN54 complex in PCH type 4 lead to a more severe clinical phenotype in comparison to a missense mutation in PCH2A, a connection between severity of gene mutation and clinical phenotype can be suggested (Namavar et al., 2016). Overall, developing neurons appear more susceptible to disruption of protein synthesis, as high demand occurs during neurogenesis (Namavar et al., 2011b).

Children with PCH type 2<sup>1</sup> display severe motor and cognitive impairment from birth. Children suffer predominantly from early-onset dyskinetic movement disorder with spastic elements and little or no gross motor development (Namavar et al., 2016; Steinlin et al., 2007 Sánchez-Albisua et al., 2014). Higher cognitive functions are almost absent but some development of communicative functions is observed (Sánchez-Albisua et al., 2014). Feeding and drinking difficulties are reported in almost all cases (Graham et al., 2010; Sánchez-Albisua et al., 2014; Steinlin et al., 2007), requiring gastrostomy for parenteral feeding, improving overall survival (Namavar et al., 2016). Severe, mostly therapy resistant epilepsy, in several cases developing into status epilepticus, have been widely observed (Sánchez-Albisua et al., 2014).

PCH type 2 patients have been reported to suffer from central visual impairment, although in the absence of primary optic nerve atrophy, which is a criterion for PCH3 (Namavar et al., 2011b). When investigating on the natural course of the disease in more detail, however, nearly 90% of children develop fixation and following with the eyes, although delayed (Sánchez-Albisua et al., 2014). Also, spinal anterior horn cells have not been found to be affected in any case of PCH type 2 post-mortem, further differentiating from PCH type 1 (Namavar et al., 2011a).

---

<sup>1</sup> PCH2A subtype has not been implemented in clinical practice sufficiently, thus the broader classification of PCH type 2 is referred to.

In particular during infections, children with PCH type 2 are more susceptible to complications such as dehydration (Namavar et al., 2016) and in more severe cases even exacerbation of subclinical rhabdomyolysis, indicated by elevated levels of creatine kinases (Barth et al., 2008; Uhl et al., 1998). Other complications, such as malignant hypothermia, have also been reported (Namavar et al., 2011b).

Life expectancy is difficult to determine as patients suffer from crib death early in life (Namavar et al., 2016), or death in the first year of life (Steinlin et al., 2007). In most cases, children do not reach puberty (Namavar et al., 2011a) and the study on natural history of the disease indicated that more than 50% of affected children die before the age of 10 years (Sánchez-Albisua et al., 2014). However, there has been a report of one patient alive at 31 years of age (Namavar et al., 2011a).

Defining neuroimaging features (MRI) are a hypoplastic ventral pons and a hypoplastic cerebellum with significantly reduced cerebellar hemispheres and comparably intact vermis and floccule resembling a dragon-fly like structure (Barth et al., 2007; Goasdoué et al., 2001; Graham et al., 2010; Uhl et al., 1998). However, deducing clinical outcome from MRI status has been refuted (Steinlin et al., 2007).

During pregnancy, there is usually no indication for brain abnormality in the foetus (Sánchez-Albisua et al., 2014), in rare cases mothers may present with polyhydramnios (Budde et al., 2008; Steinlin et al., 2007), however these cases are mostly associated with PCH4 (Steinlin et al., 2007). Tractography on prenatal MRI indicated a lack of pontine crossing fibres, highlighting a possibility to detect pontine defects in-utero (Graham et al., 2010). In high-risk pregnancies, genetic testing is recommended (Graham et al., 2010).

Differential diagnosis for pontocerebellar defects include children with extreme prematurity as well as metabolic disorders such as glycosylation defects (Johnsen et al., 2005; Steinlin et al., 2007). Disruption during cerebellar development in the foetus or the very preterm born child may result in an acquired phenotype of pontocerebellar malformation, on MRI indistinguishable from PCH (Messerschmidt et al., 2005).



Treatment for children with PCH type 2 centres on symptomatic approaches such as supporting impaired swallowing and preventing malnutrition by performing percutaneous endoscopic gastrostomy or respiratory support during infections (Namavar et al., 2011b).

### **1.3 Brain development in PCH2A**

Unravelling the genetic basis of PCH2A in recent years (Budde et al., 2008; Namavar et al., 2011b), has shed a new light on the role of RNA splicing defects in brain development, especially cerebellar development. Clinical presentation and neuropathological analysis outline the developmental characteristics in children with pontocerebellar hypoplasia type 2.

#### **1.3.1 Neurological presentation in PCH2A**

Signs for a developmental defect already become apparent in the first week of life in most children with PCH (Steinlin et al., 2007). At birth, children are normocephalic (Sánchez-Albisua et al., 2014), however always below the 50<sup>th</sup> percentile (Namavar et al., 2016). Signs for disruptive brain development emerge as children show a progressive microcephaly with head circumference developing to -5.5 standard deviation at five years of age (Sánchez-Albisua et al., 2014).

It has been argued that PCH2A is characterized by early neurodegeneration, especially affecting the cerebellum, followed by some developmental progress. As in the study on natural history, children made some basic developmental progress and only 10% of patients lost functions, they previously acquired. However, severe motor deficits are present as milestones of crawling, standing, walking or talking are not reached (Sánchez-Albisua et al., 2014).

#### **1.3.2 Neuropathological findings in PCH2A**

Based on Barth et al., 2007, unless otherwise referenced.

Neuropathological findings in PCH type 2 indicate neurodegenerative changes in infratentorial and supratentorial structures, the latter being significantly less affected.

For pons, the ventral proportion has been reported to be severely affected showing extensive neuronal death (Namavar et al., 2016). On the contrary, pontine tegmentum, composed of the long motor and sensory tracts, is unaffected. Overall, transverse pontine diameter is reduced up to 50% solely due to loss of the ventral compartment.

Reported structural pathologies in cerebellum comprise reduced and dorsoventrally flattened hemispheres with an almost intact vermis, leading to the typical dragon-fly impression to the cerebellum. Short unbranched cerebellar folia, reminiscent of hypoplastic changes on the one hand and short folia in reduced number on the other, were found. Loss of purkinje and granule cells in circumscribed segments was interpreted as indication of cerebellar disruption at around 25 weeks of gestation.

Most degenerative signs, such as sharply demarcated areas, where cerebellar cortex lost its full thickness, are thought to result from regression at an early stage of development (Ekert et al., 2016). Additionally, segmental loss occurs in the nuclear systems of the cerebral cortex, dentate nucleus and inferior olivary nucleus, all three interlinked by the climbing fibre system.

In one patient, regressive changes in the form of cyst formation in cerebellar white matter and vascular changes with intimal proliferation and splitting of elastic interna have been observed. Also, wide-spread gliosis in the cerebellum suggests an ongoing degenerative process.

Unspecific signs are described for supratentorial structures with neuronal loss in the cerebral cortex. Additionally, regressive elements in the frontal lobe in the form of gyral atrophy have been found but myelination was unaffected.

#### **1.4 Genetic testing**

Previous studies (Namavar et al., 2011b; Sánchez-Albisua et al., 2014) applied genetic testing to select a homogenous group from the heterogenous pool of PCH type 2 patients. The missense p.A307S mutation in the *TSEN54* gene (Budde et al., 2008; Namavar et al., 2011b) has been identified as the most prevalent pathogenic mutation in the *TSEN* gene in PCH type 2, hence defining a homogenous cohort of patients based on genetic testing.

## **1.5 Magnetic resonance imaging (MRI) in PCH type 2**

### **1.5.1 A non-invasive imaging tool: MRI**

Magnetic resonance imaging (MRI) provides the ability for non-invasive 2D or 3D reconstruction, particularly suited for assessing brain development (Tocchio et al., 2015). Since there is no risk to the child or, in the application of prenatal testing, to its mother, MRI imaging provides the gold standard for an indirect visualisation of neuroanatomy in children (Lerch et al., 2017).

In the context of PCH, MRI is applied for primary diagnosis of pontine and cerebellar malformations (Namavar et al., 2011a). Since at least one MRI scan is performed in children with PCH type 2, MRI data is widely available in an otherwise orphan disease. Thus, substantial imaging data can be aggregated to analyse brain development in a small-sized cohort.

Assessing regional volume changes allows inference about development in specific brain structures (Dennis and Thompson, 2013). Plotting brain volumes in a cross-sectional analysis, provides sufficient data to deduce brain development in children with PCH type 2. In addition, longitudinal data may be examined.

MRI data in PCH is heterogenous in format and quality, requiring manual segmentation over a (semi-)automated approach. In any case, manual segmentation is regarded as the most accurate method for volumetric analysis in MRI (Despotović et al., 2015).

### **1.5.2 MRI findings specific to PCH type 2**

On MRI, severe ventral pons and cerebellar hemisphere hypoplasia are the striking features of PCH type 2. Infratentorial structures feature diminished cerebellar hemispheres with the exception of vermis and floccule (Namavar et al., 2011a), lending resemblance to a dragon-fly like cerebellum in the coronal plane. Dilatation in cerebromedullary cistern and fourth ventricle are observed in later stages of PCH (Steinlin et al., 2007). The hypoplastic cerebellum exhibits varying degrees of atrophy (Namavar et al., 2016) on MRI, in regard to the age of the patient. Atrophy in the ventral pontine compartment seems to be progressive

in later stages of the disease hinting a regressive development in PCH type 2 (Namavar et al., 2011b, 2016).

Accounts on supratentorial structures for patients with PCH type 2 vary from unremarkable (Namavar et al., 2011a) to mild cerebral atrophy and ventriculomegaly (Steinlin et al., 2007). Dilatation has been reported for third ventricle, frontal horns (Steinlin et al., 2007) and outer CSF space (Namavar et al., 2011b, 2016). Structural deficits concerning the cerebral cortex show reduced white matter on frontal horns and simplified gyral patterns in the frontal lobe (Steinlin et al., 2007). On follow-up, mild progressive supratentorial atrophy has been found in two cases of PCH type 2 (Steinlin et al., 2007). Myelination is delayed, however no extensive demyelination occurred (Namavar et al., 2011a). Structural defects found in other neurodegenerative diseases have not been observed, i.e. no corpus callosum defect (Uhl et al., 1998).

## **1.6 Aims and Hypothesis**

"A main feature of PCH2A is a severe microcephaly during development. At birth, most affected children are normocephalic and supratentorial brain imaging is - in contrast to cerebellum and pons - reported as unremarkable. The postnatal pronounced progressive microcephaly may have two explanations: 1) the cerebellum establishes millions of projections to the telencephalon, especially to the frontal lobe (Middleton and Strick, 1998; Trepel, 2008) during foetal and early infantile life. PCH might disturb this development. In this case, a reduced growth of the telencephalon, especially the frontal lobes would be expected; 2) on the other hand, an ongoing neurodegeneration might also play a role. Evidence of telencephalic volume loss indicating brain atrophy at later ages would support this hypothesis.

Volumetric MRI analysis allows the in-vivo quantification of brain development. The aim of this study was to analyse intracranial volumes in a genetically homogeneous group of children with PCH2A, e.g. all carrying the missense mutation (p.A307S) in the *TSEN54*-

gene. This could provide some insight into the impact of the gene defect involved and its protein product in relation to brain function and development."<sup>2</sup>

---

<sup>2</sup> The main results of this work have been published with the doctoral student as first author (Ekert et al. 2016).

## **2. Method**

The method was first published in Ekert et al., 2016.

### **2.1 Patients**

Patient MRI data were obtained in the context of the preceding clinical PCH2A study: Natural course of pontocerebellar hypoplasia type 2A (Sánchez-Albisua et al., 2014). The protocol for collecting patient data (Sánchez-Albisua et al., 2014) consisted of contacting PCH2A families through the PCH2A parents' organisation in Germany and Switzerland. A standardised questionnaire was sent to parents and answered via a standardised telephone call from the researchers. Parents were asked to submit MR images to the research team for further information. The collected MRI data on film as well as in digital DICOM format were the basis of this investigation.

Subjects were included if they met the clinical, neuroradiological features as well as positive molecular testing for the homozygous mutation 919 G>T, p.Ala307S in the *TSEN54* gene. Clinical diagnosis were defined as “primary developmental disorder with dyskinetic/spastic movement disorder” in addition to neuroradiologic findings in MRI consisting of “pontocerebellar hypoplasia with dragonfly-like configuration of cerebellar hemispheres”(Sánchez-Albisua et al., 2014). Parents gave informed written consent. The study was approved by the University of Tübingen ethics committee (no. 105/2012BO2).

### **2.2 MRI data**

#### **2.2.1 Patient MR images**

Thirty-six MR images from 27 children with PCH2A were collected either on film or as digital copy in DICOM format. Four MRI scans had to be excluded for one of the following reasons: Either the MRI films did not contain a measurable scale (n=3) or the sequence did not cover the entire brain for volumetric analysis (n=1). Since only one MRI scan per patient was accepted, eight MRI scans were excluded (the latest MRI scan was chosen). As a result, 24 MR images of 24 children with PCH2A remained for further analysis. The excluded 12 MRI scans were not discarded, but instead used for longitudinal analysis (Ekert et al., 2016).

Gender was almost evenly distributed with 11 males and 13 females. The age range was 0.02 to 17.06 years with a median of 0.81 years and a mean of 2.41 ( $\pm 0.83$ ) (95% confidence interval 0.6969-4.1286). The histogram below illustrates most patients (n=20) having their last scan between birth and up to four years of age (Ekert et al., 2016).

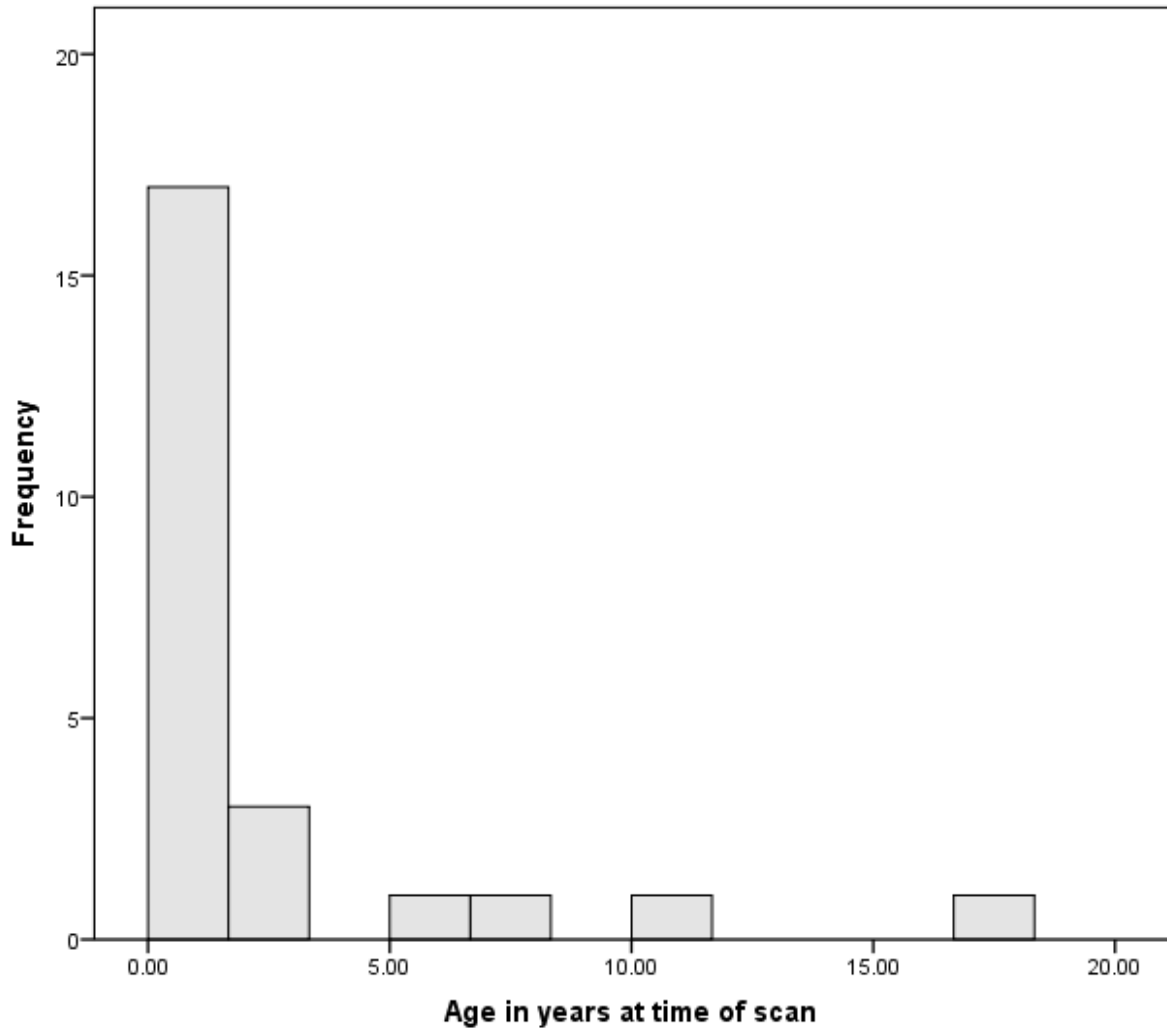


**Figure 2-1: Histogram of Age Frequency in PCH2A patients.** *Illustrating age distribution of 24 PCH2A patients with most patients (n=20) having their scan between birth and up to four years of age.*

Conventional MRI of children with PCH2A consisted of T1-, T1-IR, T2-, and FLAIR-weighted sequences acquired in different planes (see appendix for details) with overall high in-plane resolution and a mean slice thickness of 4.41mm ( $\pm 1.94$ mm). Four children had high-resolution T1-weighted images with a voxel size of 1x1x1mm (n=2) and 0.5x0.5x1.3mm, 0.9x0.9x1.0mm respectively. Regrettably, the high in-plane-resolution could not be chosen in all four children.

**Table 2-1: MRI sequence and resolution details for children with PCH2A (Ekert et al., 2016).** *Table is read horizontally. Frequency of the different MRI sequences are shown above slice thickness in their axial, coronal and sagittal plane with total number of scans in the right-hand column.*

<b>plane</b>		<b>T1</b>	<b>T2</b>	<b>FLAIR</b>	<b>T1-IR</b>	<b>Total</b>
<b>axial</b>	number	13	3	0	6	22
	slice thickness mean	5.25mm ( $\pm$ 1.67mm)				
<b>coronal</b>	number	8	8	2	2	20
	slice thickness mean	4.36mm ( $\pm$ 2.01mm)				
<b>sagittal</b>	number	11	6	0	0	17
	slice thickness mean	3.47mm ( $\pm$ 1.68mm)				

### 2.2.2 Longitudinal analysis in five patients

Longitudinal analysis was performed in five patients consisting of three males and two females; one female patient providing four consecutive scans. In the main cross-sectional comparison of this study, the follow-up scans had to be excluded and were thus examined in longitudinal analysis. Overall, 13 scans were plotted with corresponding volume over age in years. The charts were analysed on a visual basis to confirm volume trends found in cross-sectional analysis. The age range at time of scan proved to be 0.02 to 11.38 years.

One female patient (pat\_2) provided four scans from 0.04 to 1.97 years of age. Since PCH2A children rarely receive more than one scan, special attention was paid to her consecutive development.

Only one patient had a long-term follow up scan at 11 years of age with examinations at 5 months and 11 years of age.

### 2.2.3 MRI data of healthy controls

Controls of typically developing children were compiled from the National Institute of Health Pediatric MRI <sup>3</sup>Data Repository (Evans and Brain Development Cooperative Group,

---

<sup>3</sup> National Institute of Health Pediatric MRI Data Repository Version 5 (2012) (OMB number: 0925-0667)



2006)<sup>4</sup> comprising “554 unседated medically healthy, psychiatrically normal children and adolescents/young adults” (Evans and Brain Development Cooperative Group, 2006).

For each PCH2A patient a corresponding age and gender-matched control was chosen, which resulted in equivalent gender and age distributions with 13 females and 11 males in the control cohort: median 0.79 years (95% confidence interval 0.7006-3.9327, range 0.02-16.08 years). Such gender-matched controls limit the effect of difference in inter-gender brain volume development.

All control MR images were compromised of T1 sequences with high in-plane resolution: mean voxel size 1.01mm ( $\pm 0.01$ ) x 0.99mm ( $\pm 0.01$ ) x 2.82mm ( $\pm 0.10$ ).

Volumetric analysis assessed digital MR images (DICOM) in the same manner as analogue MRI films; the method was only modified in the first step: converting all data to digital format (figure 1.3). First, a manual mask of the desired brain area was created by manual segmentation, second, the mask was refined by setting an intensity threshold. Setting a threshold ensured removal of cerebral spinal fluid (CSF) signal, thus resulting in the volume of the desired brain structure. This two-step manual processing allowed for comparable analysis of digital MRI scans (DICOM format) using ITK-SNAP (Yushkevich et al., 2006) as well as analogue MRI films (JPEG stack combined in tiff format) using ImageJ (Schneider et al., 2012) software. Different image-file formats called for different programs to analyse mask area, however each program achieved volume measurement in the same manner.

---

<sup>4</sup> Statement regarding use of NIH data: Data used in the preparation of this dissertation were obtained from the Pediatric MRI Data Repository created by the NIH MRI Study of Normal Brain Development. This is a multi-site, longitudinal study of typically developing children, from ages new-born through young adulthood, conducted by the Brain Development Cooperative Group and supported by the National Institute of Child Health and Human Development, the National Institute on Drug Abuse, the National Institute of Mental Health, and the National Institute of Neurological Disorders and Strokes (Contract #s N01-HD02-3343, N01-MH9-0002, and N01-NS-9-2314, -2315, -2316, -2317, -2319 and -2320). A listing of the participating sites and a complete listing of the study investigators can be found at [http://www.bic.mni.mcgill.ca/nihpd/info/participating\\_centers.html](http://www.bic.mni.mcgill.ca/nihpd/info/participating_centers.html). This dissertation reflects the views of the author and may not reflect the opinions or views of the NIH.

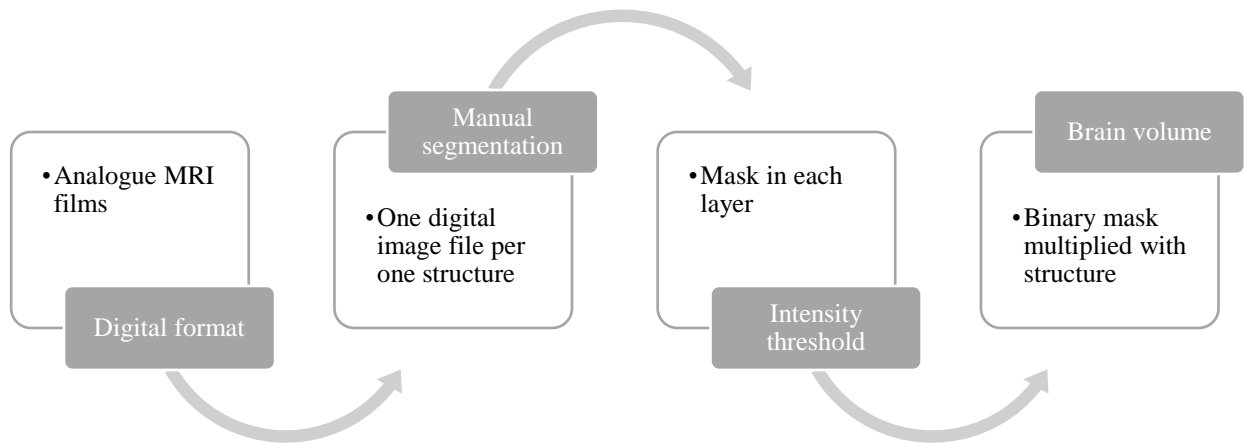


**Figure 2-2: Workflow for volumetric analysis.** First step (first box on the left) applied to MRI films only: converting analogue MRI films to digital JPEGs in tiff stack format resulting in one image file for one brain structure. After all MRI scans had been converted to digital format, the same methodology applied: Manually segmenting each layer in the specified plane, afterwards applying intensity threshold to masks resulting in binary segmented stacks. Brain volume was calculated by multiplying the binary mask with voxel volume (including an inter-slice gap, if present) in each layer.

#### 2.2.4 Analysis of digital MR images

Digital DICOM files were first converted to NIfTI format using MRtrix (Tournier et al., 2012).

NIfTI files were analysed using ITK-Snap (version 3.2, 64-bit mode). ITK-SNAP, according to its developers Paul Yushkevich and Guido Gerig, is “a software application used to segment structures in 3D medical images”(Yushkevich, Paul, 2016). One main application of ITK-SNAP, “manual segmentation in three orthogonal planes”(Yushkevich, Paul, 2016), was employed to segment the brain structures in each layer.

Before the editing process, the contrast was manually adjusted (Tools/Image Contrast). The desired brain area was manually segmented using the Polygon Tool in each layer (Main toolbox/Polygon Tool [set to continuous curve]). At the end of each volumetric analysis the mesh function was applied. The 3D-mesh structure may have indicated misplaced boundaries which stand out of the overall 3D object (update mesh). The generated mask is saved as a NIfTI file (Segmentation/Save As Image [Image file format: NIfTI File]).

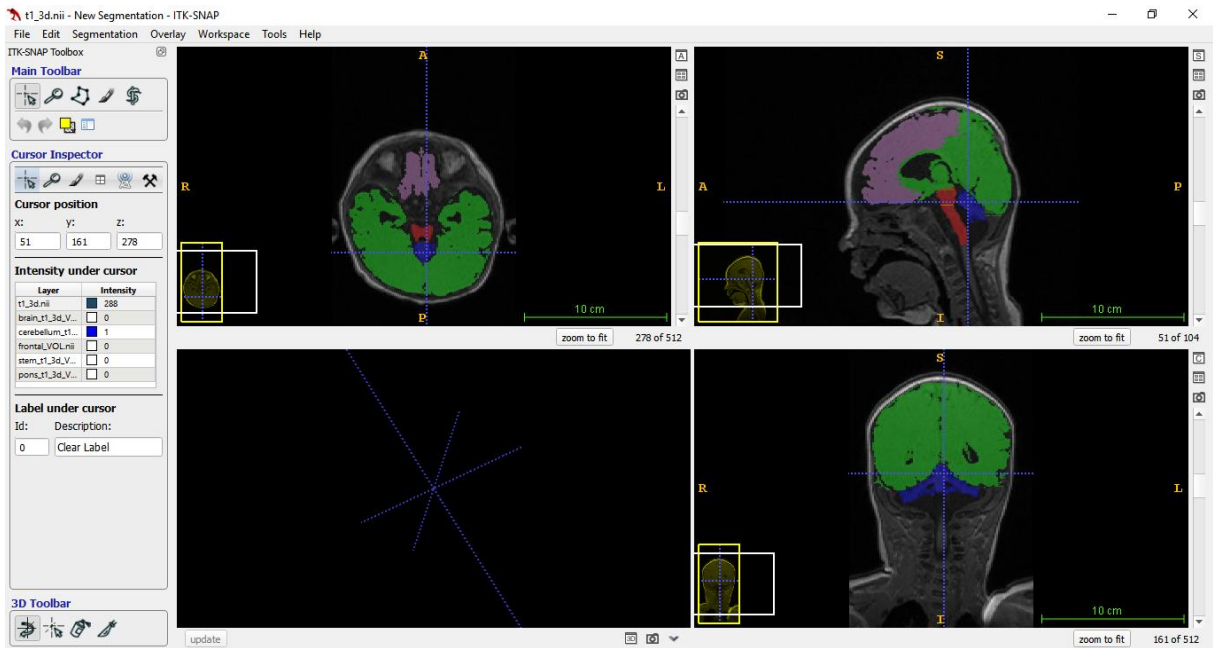


**Figure 2-3: Segmentation of brain areas in all planes (digital image processing).** Segmentation of supratentorial (green), frontal (purple), brain stem (red) and cerebellar (blue) volume is shown using ITK-Snap (Note: Pons (dark red) is shown only in axial plane). CSF signal has already been subtracted from all masks by setting the intensity threshold. For orientation, the intersection of the blue crosslines represents the same coordinates in all planes.

Finally, the mask was further refined by applying a manually set threshold reducing the higher CSF signal intensity from the binary mask, i.e. eliminating voxels from binary mask which covered CSF signal below the intensity threshold, using MRtrix (Tournier et al., 2012). The number of voxels within the binary mask was then multiplied by voxel volume (including an inter-slice gap, if present), resulting in the volume of desired brain structure.

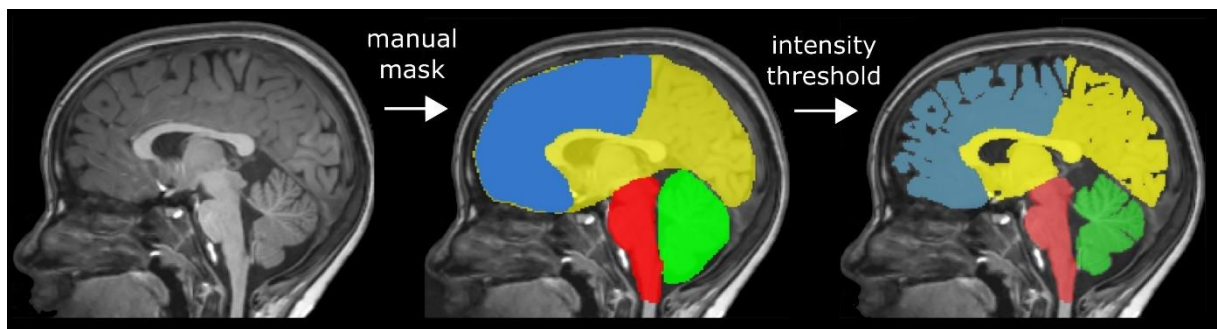


**Figure 2-4: Segmentation process overview.** For each brain area, a manually segmented mask is created (middle image). Afterwards, an intensity threshold is applied to subtract CSF signal, resulting in the desired brain volume: frontal (blue), supratentorial (yellow), cerebellum (green) and brain stem (red). (Note: Pons area is not represented in this sagittal view). First published in Ekert et al., 2016.

### 2.2.5 MRI film processing

MRI films were scanned and converted to digital image file (JPEG) by placing the films under a high-resolution camera. Each picture was taken with the same settings, keeping image resolution and lighting conditions constant.

JPEG image files in one brain structure were combined and saved in tiff (Tagged Image File Format) format, thus bundling all JPEG images in one orientation in one digital pixel-coded image file (tiff) as a stack (Image/Stacks/Images to stack).

The tiff image files of the MRI films were analysed using ImageJ (Image processing and analysis in Java) (Schneider et al., 2012) (version 1.8.0\_77 bundled with 64-bit Java). As outlined on “ImageJ features” website (Rasband, Wayne, 2016) by the U.S. National Institutes of Health, its application ranges from “display[ing] a ‘stack’ of related images in a single window” to “analysis [of] measure[ing] area” and “thresholding”(Rasband, Wayne, 2016) tiff files.

Firstly, the scale was set by measuring the displayed scale on each MRI film (Absence of scale exhibited an exclusion criterion, refer to 2.2.1) (Analyse/Set Scale). In an analogous manner to processing the digital NIFTI files, image contrast was manually adjusted (Image/Adjust/Brightness-Contrast). The desired brain area was manually segmented using the Freehand Tool (Main toolbox/Freehand selections). After the area was traced, the selection had to be saved as an overlay (Image/Overlay/Add Selection [Ctrl + B]). This procedure was reiterated until the brain area was entirely segmented in each layer of the image stack. The overlays were then imported into the ROI manager (Image/Overlay/To ROI Manager). Before a threshold was applied to the image, the initial selections were measured to assure correct deduction of pre-threshold volume from brain volume (Analyse/Tools/ROI Manager [Measure]). After the masks, here referred to as selections, were placed, the threshold was set manually in uniform manner to NIFTI processing (Image/Adjust/Set Threshold). The last step limited the volume only to threshold levels (Analyse/Set Measurements [tick “Limit to Threshold”]). The acquired brain areas for each layer were added and then multiplied with the corresponding slice thickness (adding an interslice gap if present) which was retrieved from MRI films information table, resulting in the volume of the desired brain structure.

### **2.2.6 Anatomical definition of brain areas**

First published in Ekert et al., 2016.

Brain structures were manually segmented in each designated plane, whereby available high resolution T1- weighted images were chosen.

Supratentorial brain volume was measured in the axial plane. The dura mater as well as the venous sinuses were excluded from the manual segmentation. The tentorium was defined as the caudal border as well as the caudal end of the thalamus, including the thalamus into the segmentation of the supratentorial brain volume, and excluding the optic chiasm as well as optic nerves.

Within the supratentorial brain volume, the central sulcus was identified on axial planes in order to delineate the frontal lobe from the rest of the supratentorial brain volume. The central sulcus was therefore used as the posterior border of the frontal lobe including the precentral gyrus. The lateral sulcus was defined as the lateral border, and the lateral ventricles comprised the medial borders of the frontal lobe.

The cerebellar volume was measured in the coronal plane, including the cerebellar peduncles but excluding the brain stem.

Brain stem volume was measured in the sagittal plane. The cranial boundary was represented by the diencephalon beneath the third ventricle. The cerebellar peduncles were not included. The caudal boundary was defined by the foramen magnum. The method for defining the anterior and posterior rim was adopted from a previous study (Aboulezz et al., 1985). The caudal boundary was given by the clivus anteriorly and the posterior rim was defined by the most caudal end of the occipital bone, all defined in the median of the sagittal plane.

The area of the pons was measured in the axial plane. Since the pons is not always truncated at its largest circumference, the area and not its volume was analysed. This is in part due to the large slice thickness and thus the high implication of partial volume effects. The area was set at the level of the middle cerebellar peduncles (peduncles were not included).

### **2.3 Statistical evaluation**

The data set of cerebellar, supratentorial, brain stem and frontal lobe volume [ml] in conjunction with pons area [mm<sup>2</sup>] was plotted against age in years. During statistical analysis, it was attempted to find a regression which would fit, and thus illustrate best, the relation between the independent variable age in years and the dependent variable of brain structure size in either ml or mm<sup>2</sup>.

Linear, logarithmic (with variable slopes) and square-root functions were applied to the scatter plot and their resulting R-squared value was compared. The natural logarithmic function in the form of  $y = a + b \times \ln(x)$ , where  $a$  represents the y-intercept and  $b$  the slope of the curve, was found to fit the scatter plot best with the highest R-squared value. Since only five children had more than one scan ( $n = 13$ ), only one scan per patient were considered for a valid cross-sectional analysis of brain development in children with PCH2A.

### **2.4 Validation method**

Confirming a high level of precision for two different methodological approaches was the aim of the validation process. In order to verify comparable outcomes for two methods, digital voxel files were converted to image files, i.e. DICOM files were converted to pixel-coded JPEG files.

In addition, precision was verified by intra- and inter-rater testing in five patients and controls. Intra-class correlation (ICC) and Dice Similarity coefficient (DSC) were applied to supratentorial and cerebellar volume. Choosing supratentorial and cerebellar volume measurements ensured testing the method for precision in a large as well as a small volume.

#### **2.4.1 Comparison of pixel to voxel-based method**

DICOM files ( $n=10$ ) were converted to a pixel-coded image file (JPEG). Each voxel slice was translated to a JPEG and combined into tiff stack format with an added voxel scale (one JPEG containing 50 highlighted voxels). The method then followed above-described outline

for MRI film processing, with manual segmentation of each tiff stack and setting of intensity threshold with ImageJ software.

#### **2.4.2 Intra-class correlation coefficient**

The intra-class correlation coefficient (ICC) was chosen in order to assess the level of precision in measurements for intra- (KE to KE) and inter-rater testing in two raters (KE, SG) (Shrout and Fleiss, 1979). The underlying mathematical approach following an analysis of variance.

The requirements were met with continuous data being tested for reliability in two raters. ICC provides a value between -1 and 1 where 1 represents highest group consistency and -1 the least in comparing re-measurement volume data. Thus, ICC infers the measurement conformity in intra- and inter-rater testing.

However, ICC may not be applied to compare differences in the methodological approach for voxel in contrast to pixel-coded image processing procedure (Bland and Altman, 1990), thus it was only used for validation of intra- and inter-rater testing.

#### **2.4.3 Spatial overlap Index: Dice similarity coefficient**

In the absence of ground truth in MR imaging, precision of segmented volumes was investigated using the Dice similarity coefficient (DSC) (Zou et al., 2004). DSC indicates spatial precision between segmented volumes examining variance in volumetric analysis. DSC returns values between 0 and 1, where 0 equates to no spatial overlap between measured volume A and B, and 1 highlights identical spatial overlap. It is defined as the spatial intersections between two segmentations ( $A \cap B$ ) divided by their sum and multiplied by two:

$$DSC = 2 \times \frac{A \cap B}{(A + B)}$$

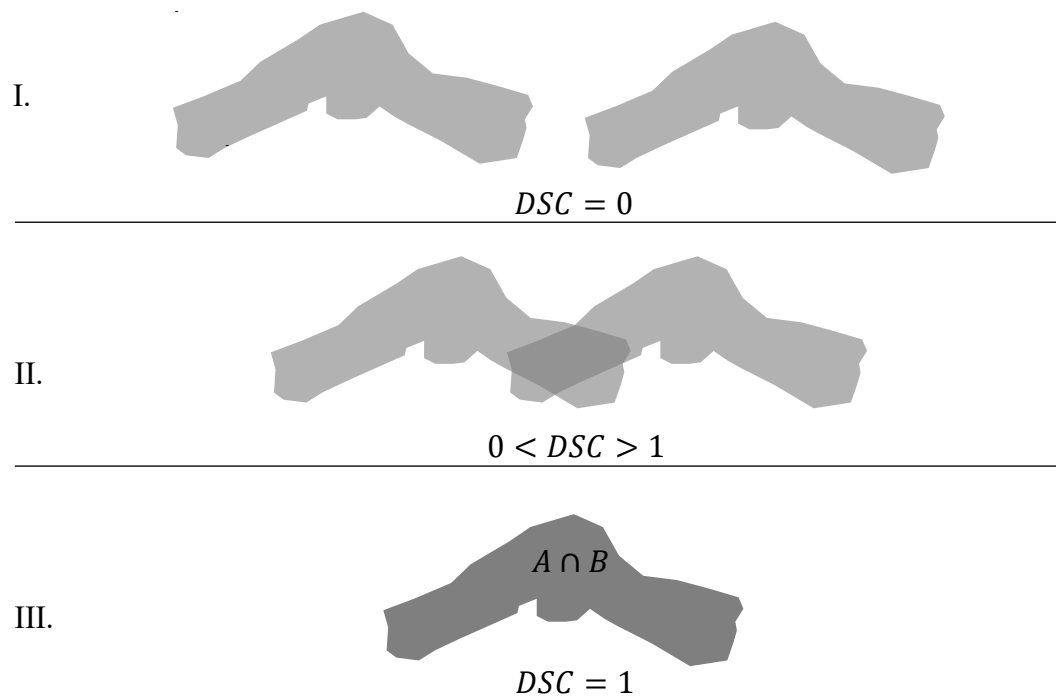


**Figure 2-5: DSC illustrating overlap in segmentation A and B.** Segmented areas resemble dragonfly feature of cerebellum as seen on MR scans in coronal plane for PCH2A. Since there is no overlap in I.  $DSC=0$ , in II. there is partial overlap ( $0 < DSC < 1$ ) and for III. there is complete spatial overlap so the intersection of A and B ( $A \cap B$ ) completely align ( $DSC=1$ ). In style of **Zou et al., 2004** (Copyright obtained).



## 3. Results

### 3.1 Volumetric results

Twenty-four patients as well as twenty-four controls were measured for their cerebellar, brain stem, supratentorial brain and frontal lobe volume; the area was taken for pons. The results can be seen in the tables below. Each brain volume was plotted against age in years at MRI scan. A suitable mathematical function was added to the scatter plot to objectify the difference in brain volume at birth as well as growth rate over the following years; the natural logarithmic function in the form of  $y = a + b \times \ln(\text{age})$ , where  $a$  represents the y-intercept and  $b$  the slope of the curve, was found to be most suitable.

### 3.2 Cerebellar volume

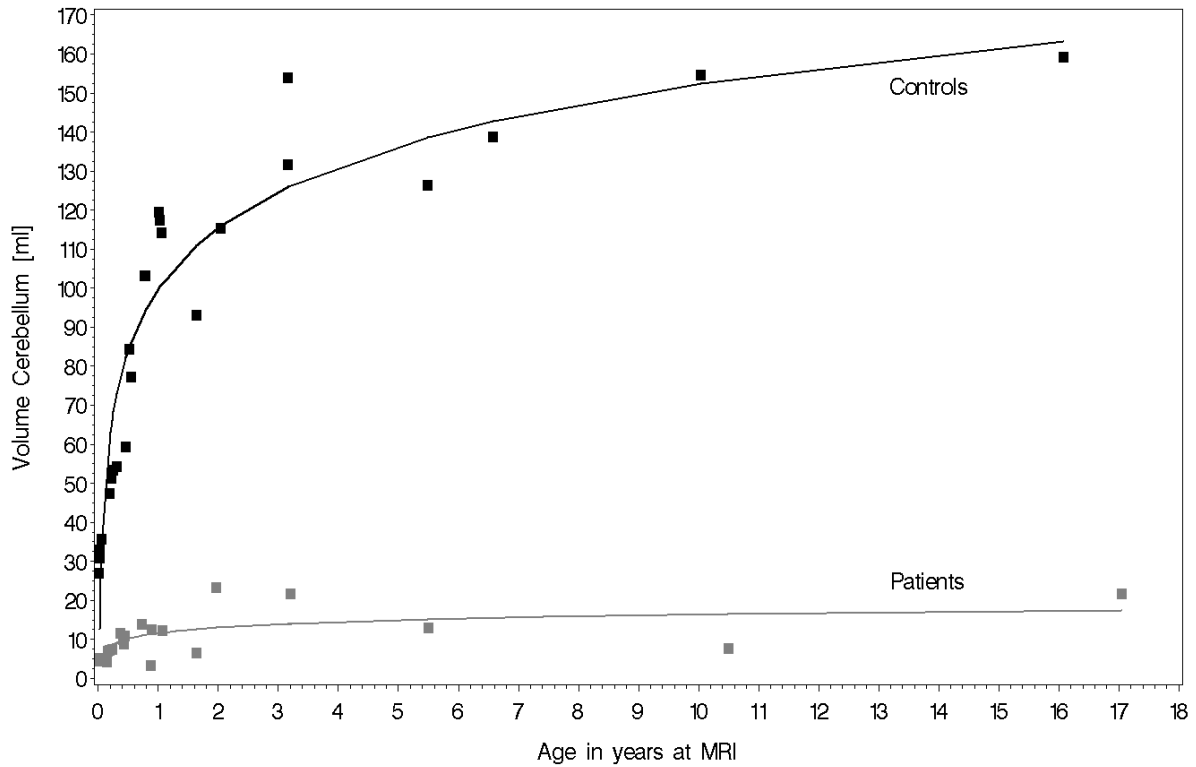


**Figure 3-1 Cerebellar volume over age in patients with PCH2A and controls.** Age in years at MRI (abscissa) was plotted against measured cerebellar volume [ml] (ordinate) comparing patients (■grey squares) to controls (■black squares). A natural logarithmic curve representing the growth curve was added for patients ( $V(pat) = 11.6 + 2.1 \times \ln(age)$ ) and for controls ( $V(cont) = 99.7 + 22.9 \times \ln(age)$ ). First published in Ekert et al., 2016.

Cerebellar volume was already significantly reduced in children with PCH2A at birth (11.6 ml vs. 99.7 ml;  $p < 0.0001$ ). Growth rate for the cerebellum was also minor with 2.1 ml/year increase against a 22.9ml/year ( $p < 0.0001$ ) increase in controls. However, cerebellar growth rate was most notable after birth but discontinued above the age of two in children with PCH2A. Cerebellar brain growth was normative in typically developing children beyond the first ten years (Brain Development Cooperative Group, 2012; Groeschel et al., 2010; Makropoulos et al., 2016; Tiemeier et al., 2010).

$$V(pat) = 11.6 + 2.1 \times \ln(age)$$

$$V(cont) = 99.7 + 22.9 \times \ln(age)$$

### 3.2.1 Brain stem volume

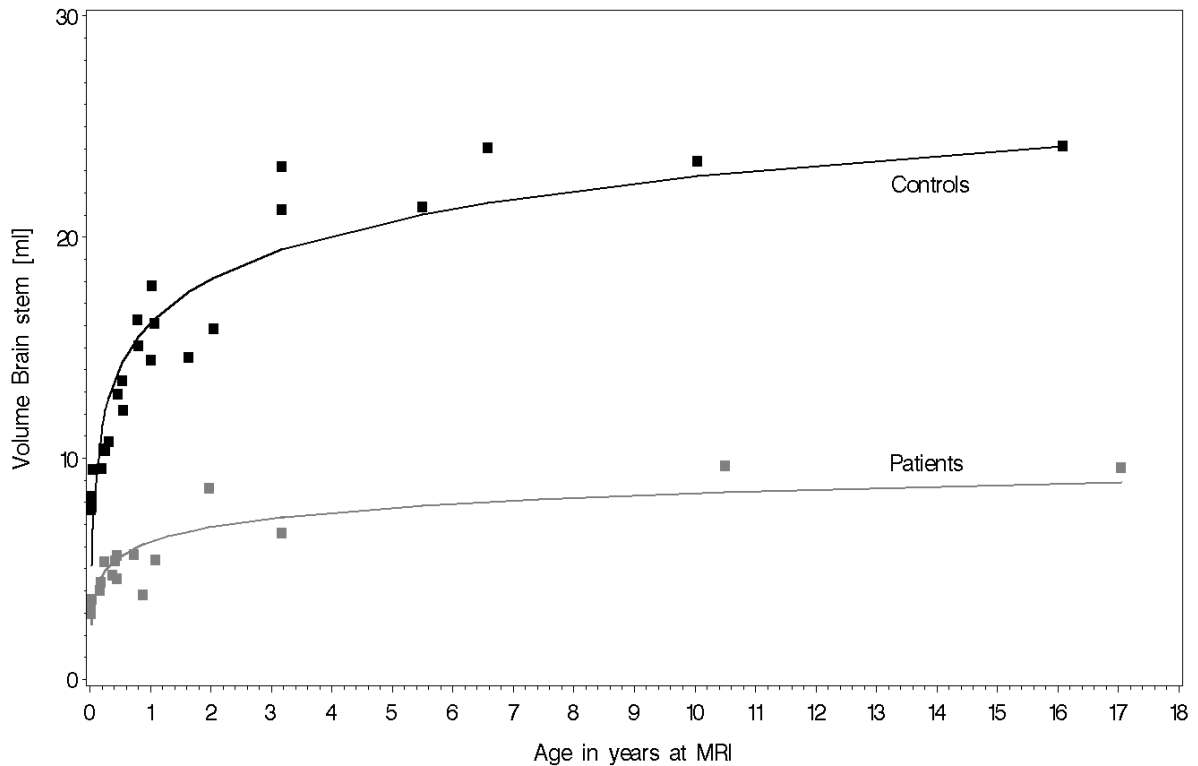


**Figure 3-2 Brain stem volume over age in patients with PCH2A and controls.** Age in years at MRI (abscissa) was plotted against measured brain stem volume [ml] (ordinate) comparing patients (■grey squares) to controls (■black squares). A natural logarithmic curve representing the growth curve was added for patients ( $V(pat) = 6.2 + 1.0 \times \ln(age)$ ) and for controls ( $V(cont) = 16.1 + 2.9 \times \ln(age)$ ). First published in Ekert et al., 2016.

Likewise, brain stem volume in children with PCH2A was already lower at birth than in typically developing children (6.2 ml vs. 16.1 ml;  $p < 0.0001$ ). Although differences at birth were quantitatively smaller due to the brain stem's overall smaller volume, children with PCH2A exhibit little growth during the first 2 years ( $p < 0.0001$ ). Following early development until age two, children demonstrated again a lower growth rate in comparison to their peers (1.0 ml vs. 2.9 ml;  $p < 0.0001$ ). Taken together, brain growth showed its highest growth rate early in life in patients and controls alike up to two years of age. For patients with PCH2A, gain in volume subsided early after two years of age to continue into a plateau compared to typically developing children.

$$V(pat) = 6.2 + 1.0 \times \ln(age)$$

$$V(cont) = 16.1 + 2.9 \times \ln(age)$$

### 3.2.2 Pons area

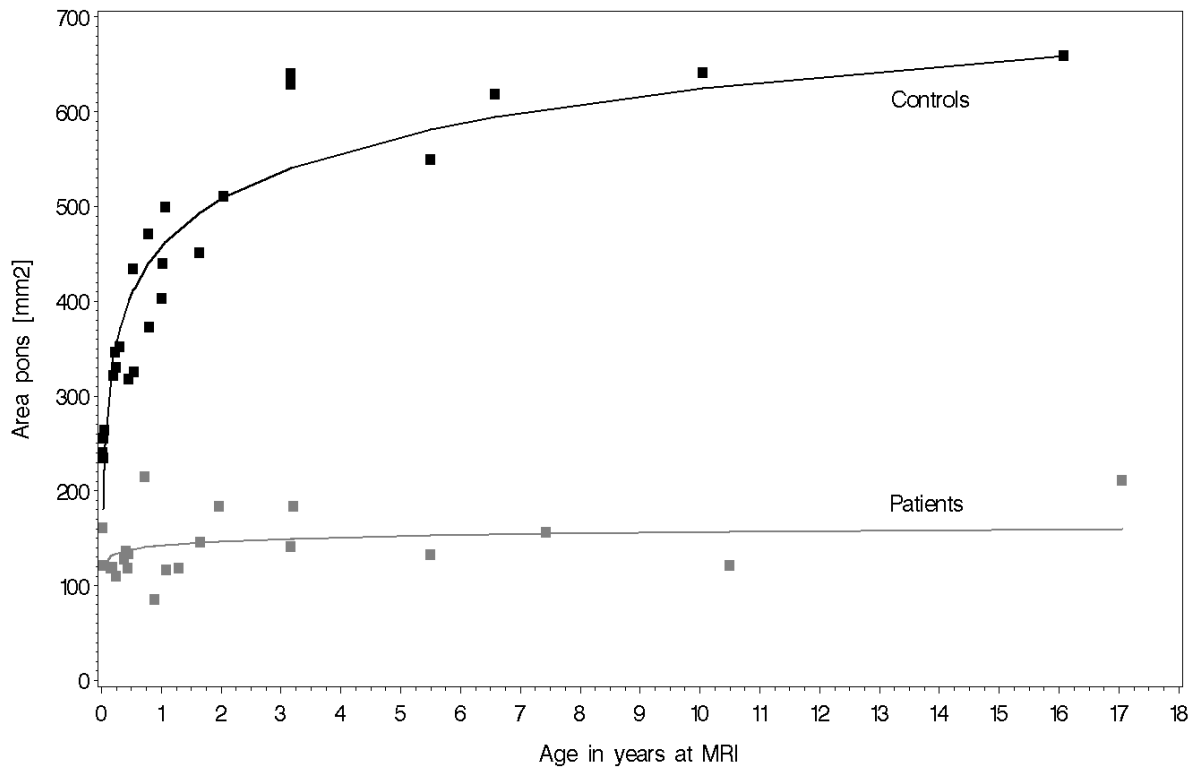


**Figure 3-3 Pons area over age in patients with PCH2A and controls.** *Age in years at MRI (abscissa) was plotted against measured pons area [mm<sup>2</sup>] (ordinate) comparing patients (■grey squares) to controls (■black squares). Area not volume was chosen for pons due to large slice thickness of MR images and thus the implications of partial volume effects. A natural logarithmic curve representing the growth curve was added for patients ( $V(pat) = 143 + 6.2 \times \ln(age)$ ) and for controls ( $V(cont) = 457 + 72.7 \times \ln(age)$ ). First published in Ekert et al., 2016.*

The area of pons was significantly lower at birth in patients (143 mm<sup>2</sup> vs. 457 mm<sup>2</sup>;  $p < 0.0001$ ) than in controls. Only a minor growth of pons area was found in patients with PCH2A (6.2 mm<sup>2</sup> vs. 72.7 mm<sup>2</sup>;  $p < 0.0001$ ) and only in the first year of life. No significant further brain growth for pons area was found thereafter in children with PCH2A. A continuous increase in pons area was shown for typically developing children well beyond ten years of age.

$$V(pat) = 143 + 6.2 \times \ln(age)$$

$$V(cont) = 457 + 72.7 \times \ln(age)$$

### 3.2.3 Supratentorial volume

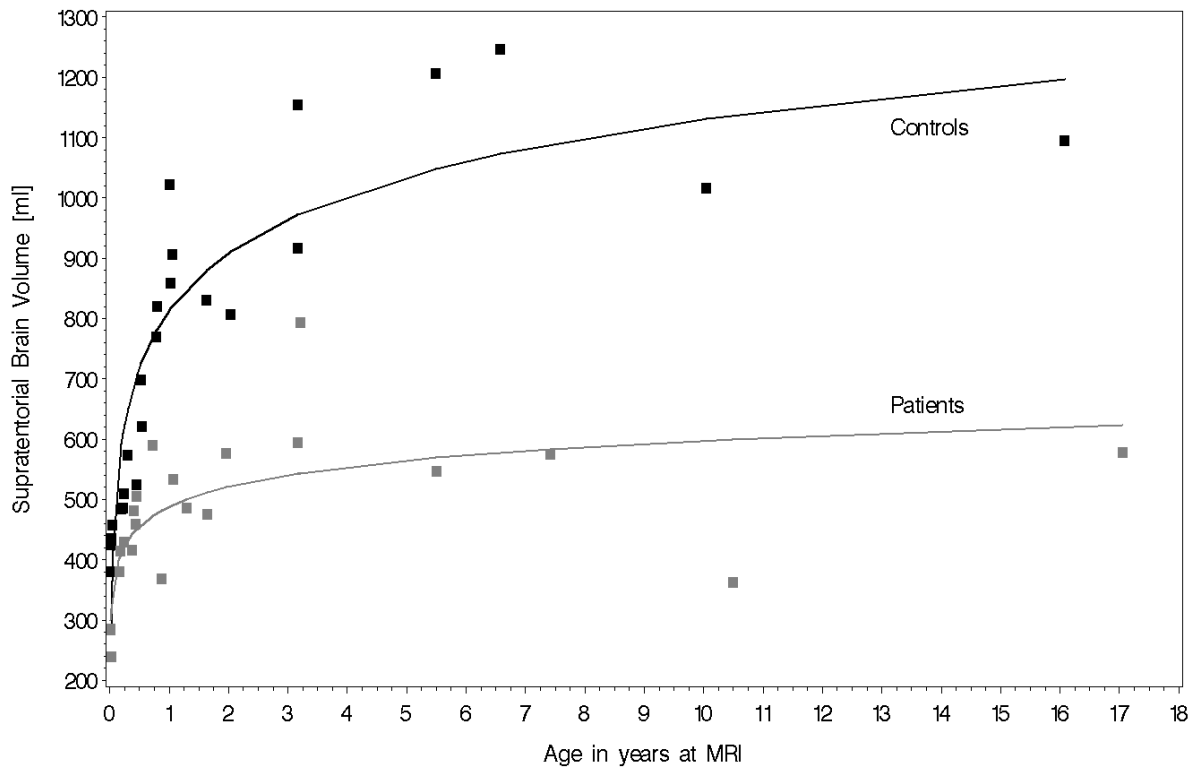


**Figure 3-4 Supratentorial brain volume over age in patients with PCH2A and controls.** Age in years at MRI (abscissa) was plotted against measured supratentorial brain volume [ml] (ordinate) comparing patients (■grey squares) to controls (■black squares). A natural logarithmic curve representing the growth curve was added for patients ( $V(pat) = 488 + 48 \times \ln(age)$ ) and for controls ( $V(cont) = 813 + 138 \times \ln(age)$ ). First published in Ekert et al., 2016.

Children with PCH2A also showed less supratentorial brain volume at birth compared to corresponding controls (488 ml vs. 813 ml;  $p < 0.0001$ ), however not as extensive as compared to cerebellar volume. The most significant brain growth was seen in the first two years of age in controls and patients, however to a significantly lesser extent in the latter (138 ml vs. 48 ml;  $p < 0.0001$ ). Beyond two years of age both groups showed continued brain growth although for patients with PCH2A to a much lesser extent. Overall differences in

brain growth and brain volume at birth between patients with PCH2A and typically developing children were not as pronounced for supratentorial brain volume.

$$V(pat) = 488 + 48 \times \ln(age)$$

$$V(cont) = 813 + 138 \times \ln(age)$$

### 3.2.4 Frontal lobe volume

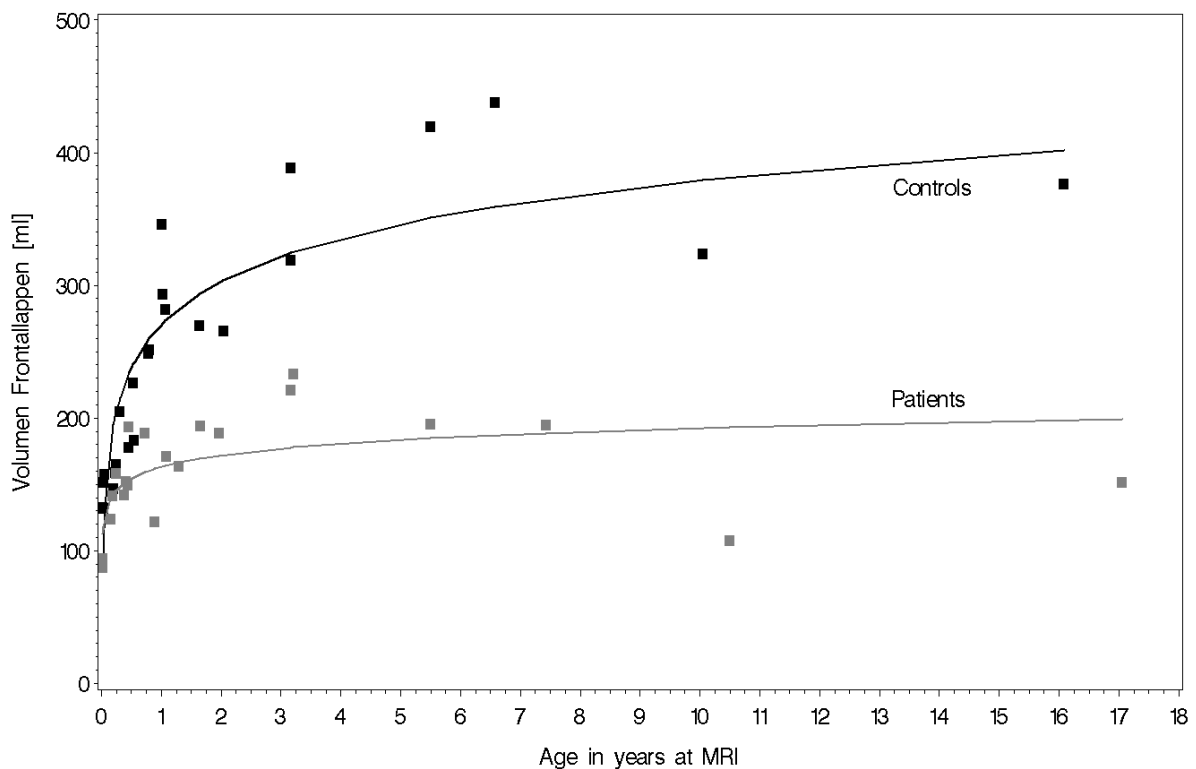


**Figure 3-5 Frontal lobe volume over age in patients with PCH2A and controls.** Age in years at MRI (abscissa) was plotted against measured frontal lobe volume [ml] (ordinate) comparing patients (■grey squares) to controls (■black squares). A natural logarithmic curve representing the growth curve was added for patients ( $V(pat) = 163 + 13 \times \ln(age)$ ) and for controls ( $V(cont) = 270 + 47 \times \ln(age)$ ). First published in Ekert et al., 2016.

At birth, patients suffering from PCH2A exhibited less frontal lobe volume compared to the NIH repository control group (163 ml vs. 270 ml;  $p < 0.0001$ ), however to a lesser extent than in all other analysed brain structures. Brain growth persisted in both groups at least up to two years of age (13 ml vs. 47 ml;  $p < 0.0001$ ), however at a lower growth rate in children

with PCH2A reaching close to a plateau phase beyond the age of two. In typically developing children, frontal lobe growth continued beyond ten years of age.

$$V(pat) = 163 + 13 \times \ln(age)$$

$$V(cont) = 270 + 47 \times \ln(age)$$

### 3.2.5 Ratio of Frontal to Supratentorial brain volume

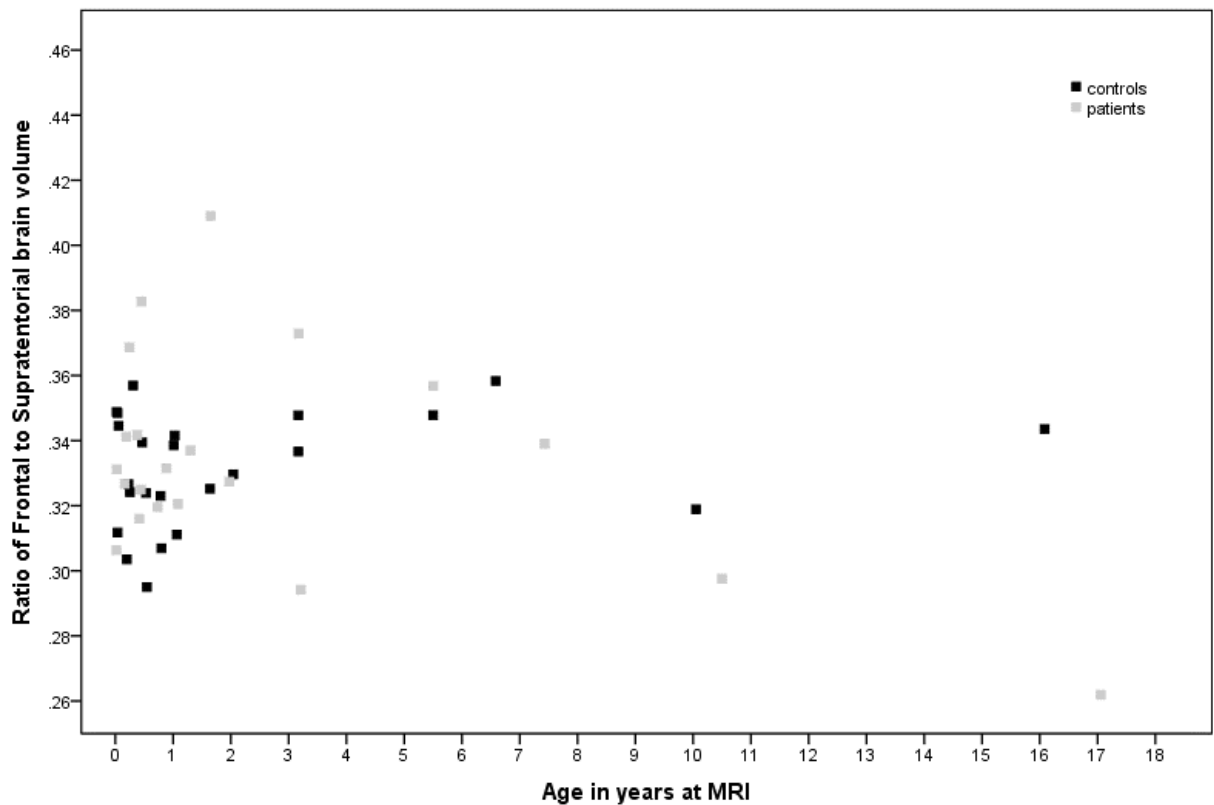


**Figure 3-6 Ratio of Frontal to Supratentorial brain volume.** Age in years at MRI (abscissa) was plotted against ratio of frontal to supratentorial brain volume (ordinate) comparing patients (■grey squares) to controls (■black squares). Frontal lobe volume was divided by supratentorial volume to investigate possible reduction in frontal lobe volume in children with PCH2A. However, there appears to be no difference in ratio of frontal to supratentorial brain volume in children with PCH2A. No regression function was added. First published in Ekert et al., 2016.

No notable difference in ratio of frontal to supratentorial brain volume was found amongst children with PCH2A compared to their corresponding controls. Neither during the first three years of life nor later in life was a substantial reduction in frontal to supratentorial

volume found. Data from three patients above the age of 8 may suggest a reduction in frontal to supratentorial ratio. However, due to the small number, no valid deduction can be made.

### 3.3 Longitudinal analysis

Visual assessment of patients longitudinal data was carried out in five patients, who provided more than one scan.

#### 3.3.1 Cerebellar volume

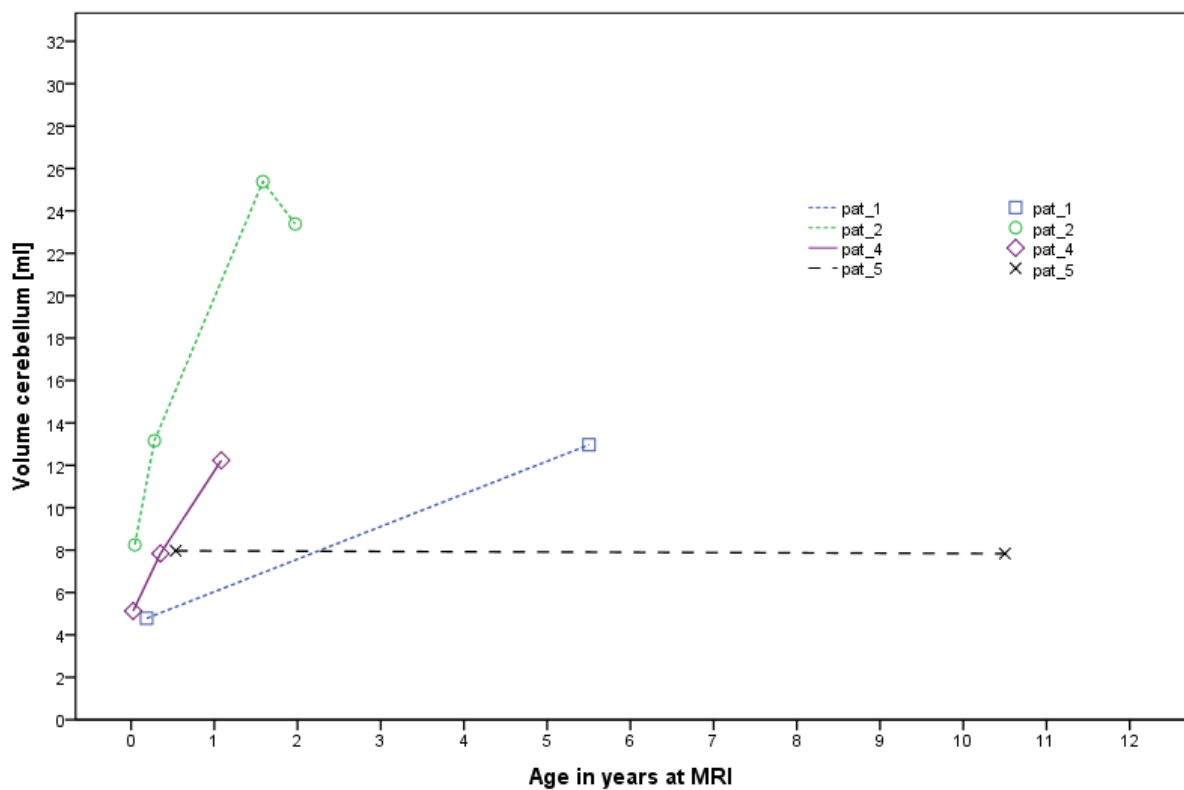


**Figure 3-7 Longitudinal analysis for cerebellar volume.** Age in years at MRI (abscissa) was plotted against cerebellar volume [ml] (ordinate) comparing longitudinal cerebellar volume trends in four patients. (Note: One patient did not provide data to assess cerebellar volume, however the patient had several scans in other brain areas. Therefore, the patient was included in the longitudinal assessment for other brain areas but is not shown in this graph). First published in Ekert et al., 2016.

Cerebellar volume increased in the first years of life in three patients. Substantial volume increase was, however, only seen in one patient (pat\_2). One patient (pat\_5) did not show any cerebellar volume growth during his development.



### 3.3.2 Brain stem volume

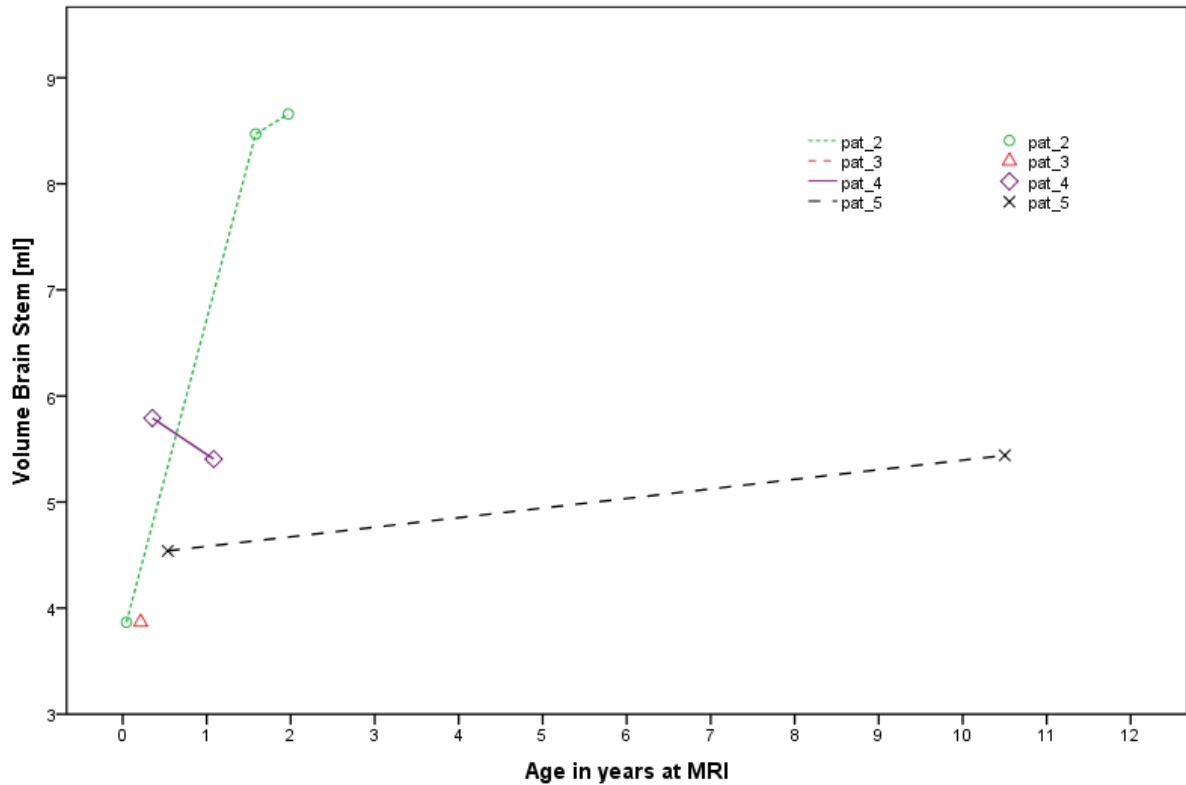


**Figure 3-8 Longitudinal analysis for brain stem volume.** Age in years at MRI (abscissa) was plotted against brain stem volume [ml] (ordinate) comparing longitudinal brain stem volume trends in three patients. Pat\_2 was provided only one data point for brain stem volume and thus could not be included for longitudinal analysis for this section. (Note: One patient did not provide data to assess brain stem volume, however had several scans in other brain areas. Therefore, the patient was included in the longitudinal assessment of other brain areas but is not shown in this graph). First published in Ekert et al., 2016.

Except for pat\_2 no volume increase was observed in longitudinal brain stem analysis. Pat\_2 showed an increase in brain stem volume in the first two years of life. Pat\_5 with one long-term follow up scan at 10 years of age showing no increase in brain stem volume. Since pat\_4's MRI scan lies within one year, no valid trends can be extrapolated from his development.

### 3.3.3 Pons area

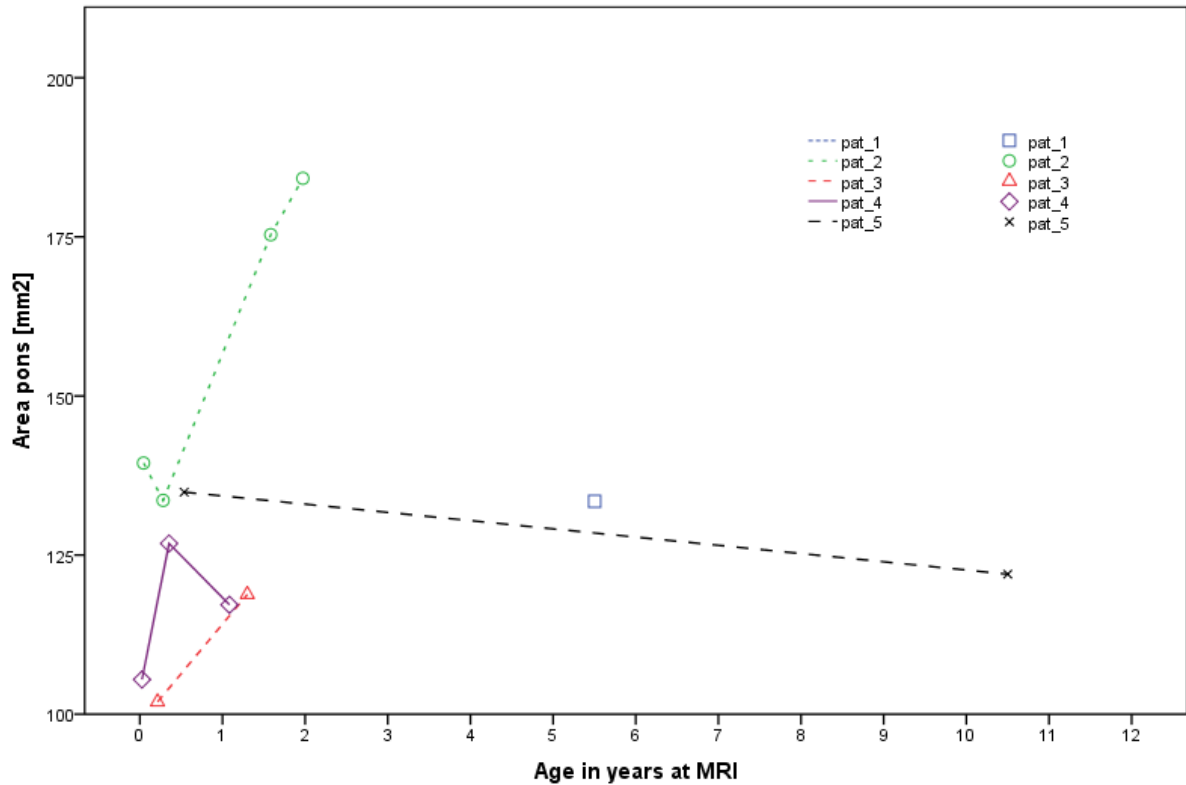


**Figure 3-9 Longitudinal analysis for pons area.** Age in years at MRI (abscissa) was plotted against pons area [mm<sup>2</sup>] (ordinate) comparing longitudinal pons area trends in five patients. First published in Ekert et al., 2016.

As in cerebellar and brain stem development, pat\_2 and pat\_5 provided similar trends: pat\_2 demonstrating an increase in pons area in the first two years of life, whereas pat\_5 showing a decline up to the age of 10 years. Unfortunately, data points for pat\_4 cannot be processed due to their inconsistent nature.

### 3.3.4 Supratentorial volume

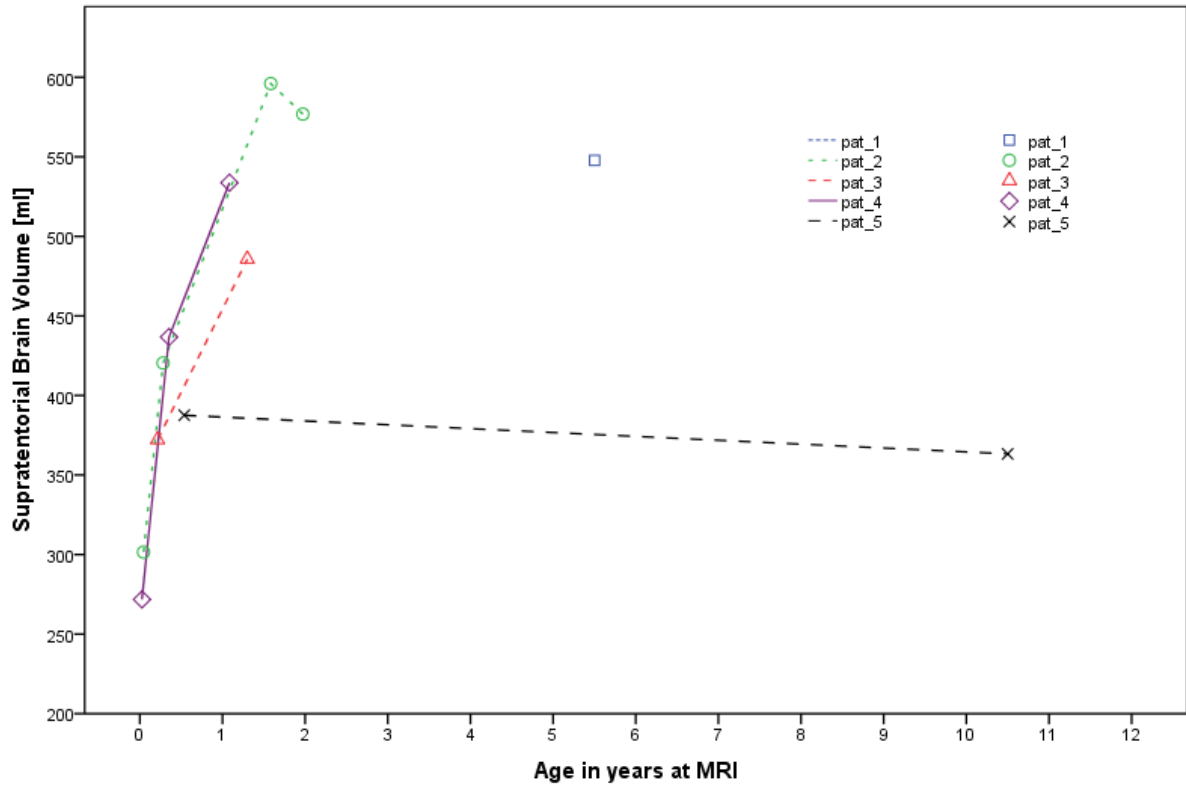


**Figure 3-10 Longitudinal analysis for supratentorial brain volume.** Age in years at MRI (abscissa) was plotted against supratentorial brain volume [ml] (ordinate) comparing longitudinal supratentorial brain volume trends in five patients. First published in Ekert et al., 2016.

Supratentorial brain volume development showed most consistency in longitudinal analysis of the five patients. A significant brain growth after birth in all but one child with PCH2A (pat\_5) was observed. A slight decrease was found in pat\_5 with less brain volume at 10 years compared to 6 months.

Most longitudinal data refer to the first 18 months. Supratentorial brain volume showed a steady increase. However, not enough data was available to make any significant statement past the first two years.

### 3.3.5 Frontal lobe volume

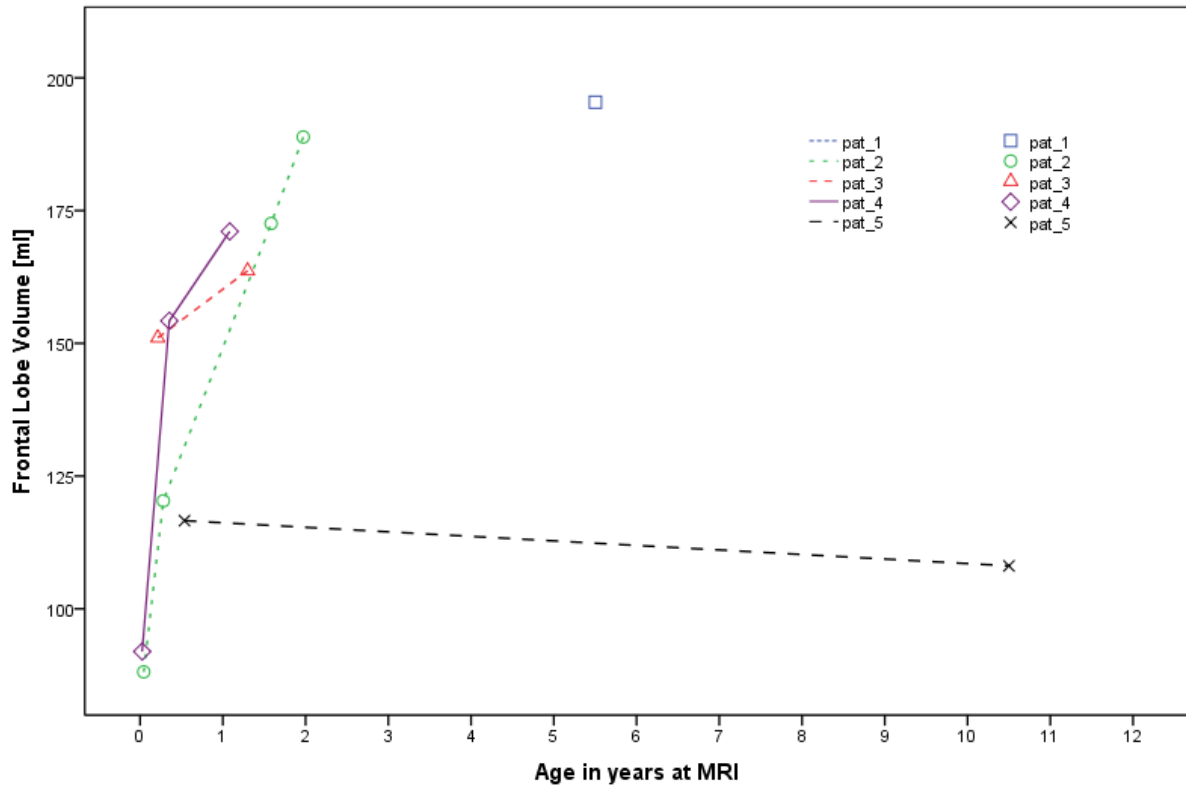


**Figure 3-11 Longitudinal analysis for frontal brain volume.** Age in years at MRI (abscissa) was plotted against frontal brain volume [ml] (ordinate) comparing longitudinal frontal brain volume trends in five patients. First published in Ekert et al., 2016.

Frontal lobe development followed the same trend as supratentorial brain development in five children with PCH2A. Patients demonstrated sufficient increase in frontal lobe volume in the first two years. No data, except for pat\_5, could be obtained after the age of two, limiting any further statements.

### 3.3.6 Exemplary development of PCH 2A in two patients

One patient (pat\_2), with three follow-up scans, reiterates the findings from the cross-sectional analysis. In the first 1.5 years of life, brain volume is increasing in all areas (see also table 3.3, pat\_2).

In one patient (pat\_5), a long-term follow-up examination at 10 years of age was available. At 10 years of age, brain volumes were smaller compared to 6 months of age with the exception of the brain stem (see table 7.6, pat\_5). The two data points do not allow, however,

to conclude a linear development without any further growth after the first examination. An alternative explanation could be that between the two data points a volume increase first happened, then followed by a decrease in the sense of atrophy, which is supported by the findings of enlargement of inner as well as outer CSF spaces on visual examination (figure 3-12).

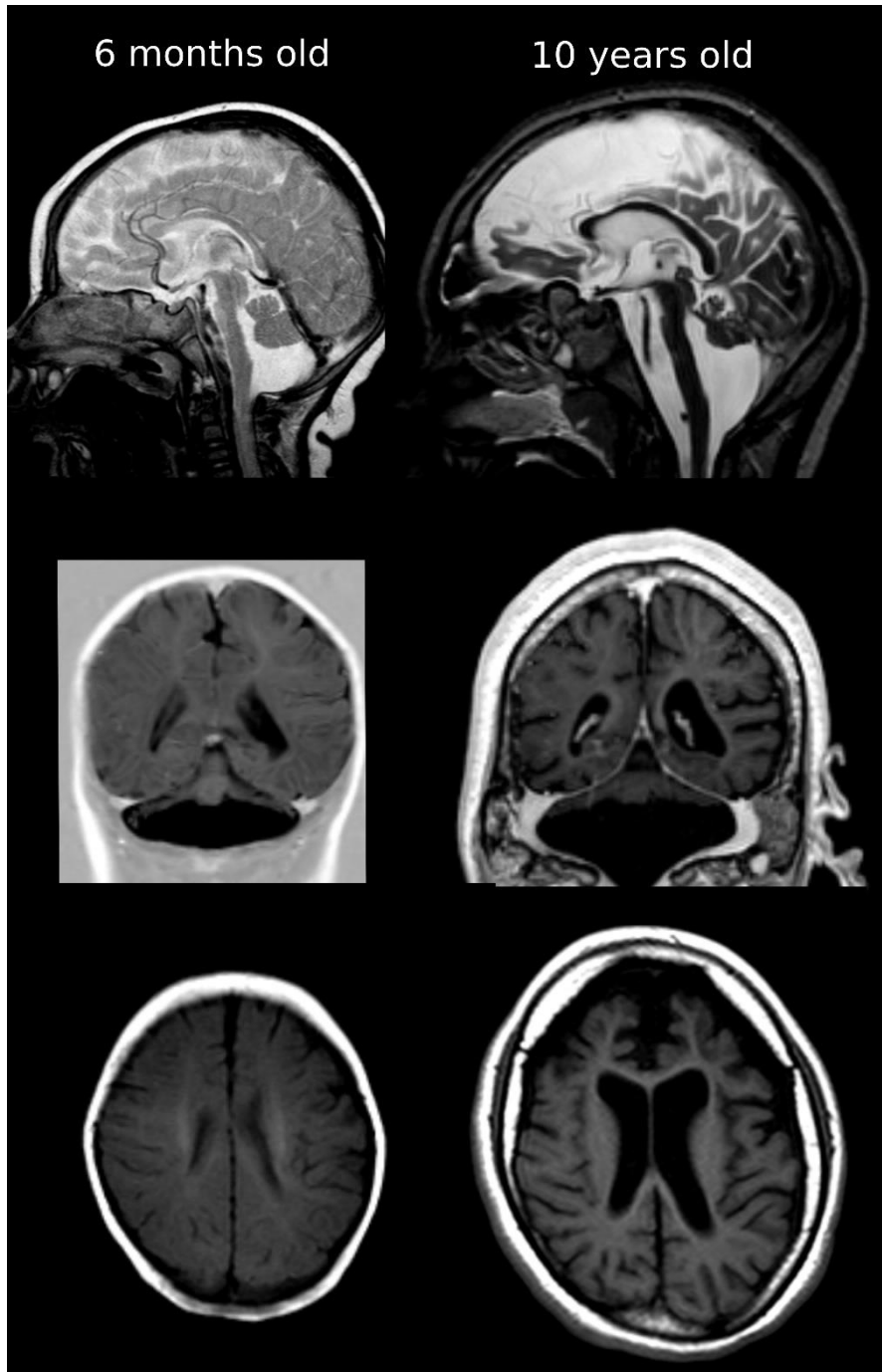


**Figure 3-12 Pat\_5 at 6 months and 10 years of age.** *Sagittal, coronal and axial scans at 6 months and 10 years of age in the longitudinal analysis in pat\_5. At 10 years of age general mild supratentorial gyral atrophy is observed, with frontal lobe more severely affected. Inner as well as outer CSF space enlarged. First published in Ekert et al., 2016.*

### **3.4 Validation results**

#### **3.4.1 Pixel contrasted by voxel processing**

Voxel MRI data sets were converted to 2D pixel format to validate pixel (MRI films) to voxel-based (digital images) volume analysis. Applying the pixel image processing method to a voxel-based data-set for supratentorial and cerebellar volume resulted in high intraclass correlation coefficient (ICC); two methods for measuring volumes concurring highly with one another.

For the supratentorial measurements ICC was 0.998 (95% confidence interval (95% CI): 0.992-0.999) and 0.998 (95%CI: 0.990-0.999) for cerebellar volume.

Note: DSC, i.e. three-dimensional overlap, can only be applied for voxel data sets. Thus, DSC was only applied to intra- and inter-rater testing however, not to voxel to pixel processing.

#### **3.4.2 Intra-rater variability**

Intra-rater testing in supratentorial and cerebellar brain structures for the primary rater KE resulted in high ICC as well as high Dice similarity coefficient (DSC) values. One rater, two measurements in the supratentorial space resulted in ICC of 0.999 (CI: 0.996-1.0) and 0.998 (CI: 0.993-1.0) ICC values in the cerebellar structure.

Additionally, spatial overlap in intra-rater testing demonstrated mean DSC values in supratentorial volumes of 0.97 ( $\pm 0.018$ ) and in cerebellar volume of 0.90 ( $\pm 0.058$ ).

#### **3.4.3 Inter-rater variability**

Inter-rater testing between KE and SG also resulted in high ICC values in the supratentorial and cerebellar space. Two rater, two measurements, showed ICC of 0.999 (CI: 0.996-1.0) in supratentorial and 0.998 (CI: 0.991-1.0) in cerebellar brain volumes.

Three-dimensional validation produced high mean DSC values in supratentorial structures of 0.98 ( $\pm 0.011$ ). Volume overlap in the cerebellar structure was slightly smaller with a mean DSC of 0.94 ( $\pm 0.033$ ).

## 4. Discussion

### 4.1 Main results<sup>5</sup>

For the first time, this study explores in detail the development of brain growth in children affected by pontocerebellar hypoplasia type 2A in measuring systematically volumes of different brain structures in comparison to normally developing children. The patients represent a very homogenous group as all carry the common p.A307S mutation in the *TSEN54* gene (Ekert et al. 2016).

The study is part of a larger project on the natural history of this condition. Analysing clinical features during the course of the disease, it was shown that affected patients all had a severe clinical phenotype with profound mental retardation, choreoathetosis, severe epilepsy, feeding problems, sleep disorders, apneas, and recurrent infections. Life expectancy was significantly reduced. Nevertheless, all children made some progress in both cognitive and motor domains, but on a low level, only 10% lost achieved abilities on follow-up (Sanchez-Albisua et al. 2014).

MRI data from 24 patients from birth up to 17 years of life, as well as longitudinal trends were evaluated for a comprehensive volume analysis. This brain morphometry assessed not only development of infratentorial but also supratentorial structures with special focus on the interaction between infratentorial brain network disruption affecting supratentorial development.

Cerebellar volumes as well as pons, and to a lesser extent brain stem volume were significantly reduced already at birth compared to healthy matched controls, reflecting severe early-onset disruption in infratentorial structures and defining the neuroradiological features of PCH. Cross-sectional analysis revealed slight growth in first two years, reaching a plateau thereafter. Slight regress for infratentorial volume was observed only in one

---

<sup>5</sup> The main results of this work have been published with the doctoral student as first author (Ekert et al. 2016).



longitudinal case later in life. Data in second decade of life was rare and thus scattered, limiting a substantial interpretation.

Supratentorial volumes, which were for most patients in the lower normal range at birth, showed a significant volume increase, especially during the first year, which was, however, less prominent than in matched controls. The difference became more important thereafter, indicating an early reduction in growth rates.

Frontal lobe was not more affected than remaining supratentorial structures. Like infratentorial development, the volume gap between patients and controls was widening during development. Cross-sectional and longitudinal analysis agreed. One case in longitudinal analysis suggested supratentorial regression in second decade of life. Unfortunately, data was also limited beyond ten years of age.

## **4.2 Context of findings**

Extensive hypoplasia in cerebellum and pons have been described as the hallmarks of PCH type 2 and is a defining feature (Barth et al., 2007; Namavar et al., 2011a; Sánchez-Albisua et al., 2014; Steinlin et al., 2007). The postnatal development of cerebellum and pons in PCH2A is reflected by the volumetric analysis in this study. In addition, for the first time we report on the fact that also brain stem is considerably hypoplastic, which was not recognised previously and thus enlarges the concept of PCH to represent global infratentorial hypoplasia, not just limited to cerebellar hemispheres and ventral pons (Barth et al., 2007; Ekert et al., 2016). The further course of the disease has been described as atrophic (Barth et al., 2007), suggesting a loss in volume after birth. However, we could show that the first two years are characterised by some volume increase in all infratentorial structures. The growth rate then subsided after the initial increase and volumes remained stable. As prenatal findings of neurodegeneration in pons and cerebellum suggests, we consider this initial volume increase followed by a plateau, which was found in the cross-sectional analysis, as well as in the longitudinal data, an important finding for PCH2A, as it does not indicate a continuum of neurodegeneration. Loss of volume was only found in one longitudinal examination later in life. Regressive elements with central pontine and cerebellar atrophy have been described in literature (Namavar et al., 2016), i.e. cerebellar changes with cyst

formation, loss of purkinje cells and vascular changes (Barth et al., 2007), however occurring in later stages of life in PCH2A. Taken together, this could indicate a late-stage regressive process in PCH2A. Infratentorial structures, although hypoplastic at birth, showed slight growth and possible late regression. In comparison, typically developing children show a continuous volume increase in infratentorial structures from birth onwards (Brain Development Cooperative Group, 2012; Ekert et al., 2016; Makropoulos et al., 2016; Tiemeier et al., 2010).

As indicated before, several studies have given evidence that morphological features of PCH develop around 22-33 gestational weeks (Goasdoué et al., 2001; Guibaud, 2004; Messerschmidt et al., 2005), suggesting a prenatal onset in PCH2A (Namavar et al., 2011b). Prenatal, and especially timely diagnosis by neuroimaging of PCH2A is difficult (Graham et al., 2010), as disruption of cerebellar development and its manifestation occurs in the second half of pregnancy.

Over the course of PCH2A, patients develop progressive microcephaly (Namavar et al., 2011a; Steinlin et al., 2007). With this study, we were able to visualise the development of brain volume underlying the microcephalic development. We found an increase in supratentorial volume up to five years of age in cross-sectional and longitudinal analysis, though at a lower rate compared to typically developing children, accounting for progressive microcephaly in PCH2A children. One patient with four consecutive scans supports the trend of initial increase with steady supratentorial brain volume growth within first 1.5 years, and only the last scan at around 2 years indicates supratentorial volume decrease. In cross-sectional analysis, supratentorial growth rate levelled successively, concurring with a progressive microcephaly, falling below  $-5.5SD$  at 5 years of age in PCH2A (Ekert et al., 2016; Sánchez-Albisua et al., 2014). Selection bias for microcephalic children can be refuted as the preceding study found 84% of patients were normocephalic at birth (Sánchez-Albisua et al., 2014).

However, data remained scarce for the second decade of life also in supratentorial volumes, impeding sufficient statements concerning regressive trends in PCH2A in supratentorial brain development. Cerebral cortex atrophy (Namavar et al., 2011a) and frontal lobe atrophy on MRI have been reported (Steinlin et al., 2007). Examining MRI scans in one case study

at 6 months and 10 years revealed enlarged inner and outer CSF space on follow-up and no increase in infratentorial and particularly supratentorial brain volumes, which can be interpreted as a regressive element in PCH2A (Ekert et al., 2016). However, limited data at a later age in this study renders these findings speculative.

### **4.3 Hypoplastic vs. atrophic brain development in PCH2 and the hypotheses of this study**

We pronounced two hypotheses for the pronounced progressive microcephaly in PCH2A postnatally: 1) Early degeneration of the - then hypoplastic appearing - cerebellum disrupts the development of network formation between infra- and supratentorial structures especially the telencephalon and the frontal lobe, with reduced growth of these structures. 2) Alternatively, ongoing neurodegeneration leads to telencephalic volume loss indicating brain atrophy at later ages (Ekert et al., 2016).

The results would further describe the impact of the RNA splicing defect in the *TSEN54* gene on the developing brain.

#### **4.3.1 Disruption of cerebellar projections**

The reduced functioning RNA protein synthesis results in a hypoplastic cerebellum as the high metabolic demand during cerebellar genesis cannot be met. Since the cerebellum establishes millions of projections to the telencephalon (Middleton and Strick, 1998; Trepel, 2008), disruption to cerebellar architecture also results in impaired supratentorial development (Ekert et al., 2016). This study found decreased supratentorial volume at birth, although less extensively than in infratentorial volume, arguing for a supratentorial disorganisation as a result from primary disruption in cerebellar development. Most notably, supratentorial brain growth was reduced compared to typically developing children, supporting the case for limited cerebellar projections secondarily disrupting supratentorial structural integrity (Ekert et al., 2016).

Cerebellar projections are abundant to the cerebral and particularly to the frontal cortex (Middleton and Strick, 1998; Ramnani, 2006; Stoodley and Schmahmann, 2009), expecting a more severely affected frontal lobe in comparison to other supratentorial structures (Ekert

et al., 2016). However, frontal to supratentorial volume ratio revealed no greater impairment in frontal lobe, particularly early in life. Later in life, scarce data limits a sufficient statement. All structures within the supratentorial volume appeared equally affected, arguing for a global disturbance to supratentorial brain architecture, not limited to the frontal cortex. Only one case study revealed some volume loss between 6 months and 10 years of age, which referred to the global and somewhat more to the frontal telencephalic volume. Cerebral atrophy has been postulated to eventually develop in all children with PCH type 2 (Namavar et al., 2011a), thus the demonstrated atrophy in this case study at 10 years of age probably resulted from progressive supratentorial depletion over time. However, the two data points do not allow to conclude a linear development, where no further growth occurred after initial examination. An alternative explanation could be that between the two data points a volume increase first happened, then followed by a decrease in the sense of atrophy, which is supported by the findings of enlargement of CSF spaces.

#### **4.3.2 Progressive neurodegeneration**

Progressive neurodegeneration with prenatal onset, accounting for the characteristic, hypoplastic pontocerebellar features, is the alternative hypothesis, which would result in a steady decrease in brain volumes. However, a progressive decline in volume was not recorded neither in infratentorial nor supratentorial structures. On the contrary, even in cerebellum and pons a slight initial increase in volume was found. In one patient with three consecutive scans in the first 1.5 years of life, a continuous volume gain was observed, discouraging the argument for a continuous volume loss in PCH2A after birth (Ekert et al., 2016).

Nevertheless, loss in volume is observed in later stages of PCH2A, as discussed above. Thus, our findings indicate that the severe prenatal neurodegenerative disruption of infratentorial brain areas is followed by brain growth even in these structures, but predominantly of supratentorial structures, although to a lesser extent than in controls, the latter supporting our first hypothesis of a negative impact for disrupted cerebellar structures on cerebral networks. This is also supported by the fact that children with PCH2A make, in the majority of cases, some developmental progress. In addition, we have some, but limited evidence, that neurodegeneration of cerebral structures resulting in atrophy happen at a later age,

which supports also our second hypothesis, however not in the sense of an ongoing but late-stage neurodegeneration (Ekert et al., 2016).

### **4.3.3 Other pathomechanisms**

PCH has first been defined with respect to the neuroimaging features of severe hypoplasia of cerebellum and pons before the underlying genetic defect could be identified. There are other pathomechanisms resulting in pontocerebellar hypoplasia in addition to these genetic causes. Extreme prematurity has been reported to result in a PCH phenotype, which is probably due to a high vulnerability of these structures for lesional mechanisms. The clinical features are, however, distinctly different and comprise mainly a subnormal cognitive development and microcephaly, and do not correspond to the complex clinical phenotype of PCH2A as discussed above (Limperopoulos et al., 2007; Messerschmidt et al., 2005). Additionally, drug toxicity has been reported to result in a PCH phenotype (Gadisieux et al., 1984; Squier et al., 1990). Hypoplasia of ventral pons and cerebellar hemispheres, resulting from either an acquired or a genetic pathomechanism (PCH), are practically indistinguishable on MR images (Messerschmidt et al., 2005). These differential diagnoses of acquired conditions are crucial with respect to genetic counselling in affected families (Messerschmidt et al., 2005).

### **4.3.4 Significance of disrupted projections**

Interrupted projections in PCH not only play a role in cerebellar-cerebral cortex connectivity, but also projections from the inferior olivary nucleus to cerebellar hemispheres are affected in PCH (Barth et al., 2007). Segmental lesions in the inferior olivary nuclear system result in the severe hypoplasia of cerebellar hemispheres as the climbing fibre system is severely impaired. This further highlights the impact of disrupted projections on the integrity of brain architecture in PCH since one functional system's demise results in another's disruption.

## **4.4 Implications of study**

For the first time, a comprehensive analysis of volumetric data in conjunction with longitudinal studies of patients with pontocerebellar hypoplasia type 2A was performed,

revealing severe volume loss in cerebellum, pons, brain stem as well as supratentorial structures at birth. Interestingly, slight volume increase was found in infratentorial brain areas during infancy. In the same manner, supratentorial areas increased in the first 5 years of life, following reduced growth and in some cases volume loss later in life. The frontal cortex was not found to be more severely affected than the rest of supratentorial structures. Reduced volumes in infratentorial as well as supratentorial brain structures argue for a hypoplastic course in pontocerebellar hypoplasia type 2A. Evidence of volume increase in the first years of life further discredit the claim of a progressive early-onset neurodegeneration, instead substantiating the argument for an early-stage disruption to brain development resulting in severe primary infratentorial hypoplasia and secondarily limiting supratentorial development. Nevertheless, volume loss was demonstrated in older patients, which is rather explained in the context of late-stage atrophy occurring in an already disturbed brain architecture (Ekert et al., 2016).

Understanding the disrupted development in children with PCH2A may form an understanding about the impact of malfunctioning RNA processing on brain development. In order to achieve further progress, the effects of molecular pathomechanism on brain architecture have to be investigated. MRI tractography may provide further insight into disrupted projections, thus further differentiating the effects of a genetic defect on inter-brain connectivity in PCH2A. In particular, MRI tractography in the context of disrupted pontine, cerebellar-cerebral and climbing fibre tracts may provide significant understanding regarding the effects of disrupted connectivity on brain function.

#### **4.5 Methodological aspects**

Heterogenous MRI data taken from different MRI scanners varying in field strength, sequences and thus resolution, proved to be one shortcoming in this study. Mostly no high-resolution MRI scans were available, increasing the impact of partial volume effects. However, it was possible to show that the measured volumes yielded high reliability and reproducibility, demonstrating that although MRI data was heterogenous, high precision was achieved. Keeping in mind, accuracy can only be approximated in the absence of ground truth on MRI scans (Ekert et al., 2016).

Also, the ramifications in comparing two- to three-dimensional data must be considered, i.e. pixel (MRI film, 2D) in comparison to voxel (digital MRI, 3D) data. Analogue signals suffer a lag of information since they do not provide information in a third axis, voxel data has a higher depth of information. For this reason, three-dimensional data-sets were converted to pixel format to assess the method's reliability in comparing 2D to 3D image data. When precision of the same sets of data were compared, high conformity in the ICC were found, arguing for the feasibility of the adopted method. Moreover, MRI Image volumetry can be applied in a 2D as well as 3D data-set (Despotović et al., 2015).

Following the same line of argument, limitations of measuring small, i.e. pons as well as large structures, i.e. supratentorial brain, may result in higher ramifications of partial volume effects on MRI. This was considered by taking the area for pons instead of its volume, resulting in high precision during the validation process (Ekert et al., 2016).

Volumetric analysis was obtained from cross-sectional examination since longitudinal data was not widely available. When comparing volume data from different patients about longitudinal trends in a disease, the interpreter may succumb to the confounder effect. To reduce the impact of confounding, a prospective cohort study would need to be carried out for brain development analysis (Groeschel et al., 2010). However, prospective studies pose new challenges, such as maintaining a constant instrumental set-up over the years as well as the low incidence rate of 1:200 000 in PCH (Namavar et al., 2011b), and thus impede prospective studies in this orphan disease (Ekert et al., 2016).

Although manual volumetry is considered the gold standard (Despotović et al., 2015), errors from lengthy contouring may arise (Collier et al., 2003). Developing an algorithm for semi-automated volumetry may provide a solution to strenuous manual volumetric assessment. Although, designing an automated process, which masters severely disturbed brain architecture, poses a complex effort, the rate of sampling patient volumes could be significantly improved while maintaining reliability with an automated process.

## 5. Abstract

Pontocerebellar hypoplasia represents a heterogenous group of early-onset neurodegenerative diseases characterised by disrupted cerebellar and pontine development, leading to a severe clinical condition with extra pyramidal dyskinesia and severe psychomotor impairment. A RNA splicing mutation has been identified in all children with PCH type 2, however its precise impact on the children's brain architecture remains unclear. To what extent cerebellar and pontine impairment affects global brain development must be investigated. Therefore, this study aimed to examine infra- and supratentorial brain volumes in a genetically homogenous cohort of patients to assess brain development of children with pontocerebellar hypoplasia type 2A.

24 patient MRI scans, obtained on film and in digital format, compared to 24 age and gender matched controls, were manually segmented for their image volume in cerebellum, brain stem, supratentorial brain, frontal lobe and pons area. All children tested positive for the missense p.A307S mutation in the *TSEN54* gene. MRI films were converted to digital pixel format (JPEG). All images received a manual mask, which was thresholded to reduce CSF signal, yielding the desired brain volume. In addition, longitudinal volume and image data in five patients were subjected to visual examination. The adapted method was validated by converting digital 3D MRI data to JPEG format as well as intra- and inter-rater testing using Intra-correlation and Dice similarity coefficients.

Volumetric data in conjunction with longitudinal case studies revealed severe volume loss in cerebellum, pons, brain stem as well as to a lesser extent in supratentorial structures at birth. This study could illustrate for the first time, a volume increase in infra- and supratentorial brain areas during infancy in PCH2A. The frontal lobe was not found to be more severely affected than the rest of supratentorial structures. Supratentorial growth continued throughout the first 5 years of life, then stagnating. No volume regression in any brain structure was seen in the first 5 years of life. The validation process revealed high precision and reproducibility as strong values for ICC and DSC in intra- and interrater were observed.

Reduced volumes in infratentorial brain structures present at birth are interpreted as the consequence of prenatal neurodegeneration leading to pontocerebellar hypoplasia. Evidence



of volume increase in the first years of life do not support the concept of a continued neurodegeneration but argue in favour of a secondary impact of these severely disturbed pontocerebellar structures on supratentorial development with microcephaly. This is supported by the evidence for some clinical progress in the first years of life in PCH2A patients. Nevertheless, volume loss was demonstrated in a longitudinal analysis in an older patient, which could be explained in the context of late-stage atrophy, eventually developing in most children with PCH.

This study provides new insight into the impact of the underlying gene defect supporting a primary cerebellar dysfunction with secondary severe disruption of cerebellar-cerebral networks and probably some late neurodegeneration.<sup>6</sup>

---

<sup>6</sup> The main results of this work have been published with the doctoral student as first author (Ekert et al. 2016).

## 6. Zusammenfassung in deutscher Sprache

Pontocerebelläre Hypoplasie umfasst eine heterogene Gruppe früh einsetzender neurodegenerativer Erkrankungen, welche primär eine Störung in der cerebellären und pontinen Entwicklung erfahren. Eine Mutation im RNA splicing Prozess im *TSEN54* Gen wurde bei allen Kindern mit PCH2A gefunden, ihre genauen Auswirkungen auf die Gehirnarchitektur bleiben jedoch unklar. Inwieweit die cerebelläre und pontine Schädigung das gesamte Gehirn beeinträchtigt, muss untersucht werden. Diese Dissertation beabsichtigte, infra- und supratentorielle Strukturen anhand des Volumens in einer genetisch homogenen Patientenkohorte zu untersuchen und dadurch Rückschlüsse auf die Gehirnentwicklung bei Kindern mit PCH2A zu erhalten.

MRT Aufnahmen von 24 Patienten, auf Folien und in digitalem Format, wurden 24 alters- und geschlechtsabgestimmten Kontrollen gegenübergestellt, um das Volumen sowohl von Cerebellum, Gehirnstamm sowie der Pons (Fläche) und gesamten supratentoriellen Volumen mit Unterteilung des Frontallappens, manuell zu segmentieren. Alle Kinder zeigten die missense p.A307S Mutation im *TSEN54* Gen. Die MRT Folien wurden in eine digitale, Pixel-kodierte Bildinformation überführt (JPEG). Anschließend wurden alle digitalen Aufnahmen manuell umfahren, ein Intensitätsschwellenwert präziserte die Maske, um überschüssige Liquorsignale zu subtrahieren. Zusätzlich wurden longitudinale Daten in 5 Patienten inkorporiert. Die Validierung der adaptierten Methode erfolgte indem 3D MRT Voxelaufnahmen in Pixel-kodierte Bilder konvertiert und vermessen wurden. Zusätzlich wurden Intra- und Interrater Tests anhand von Intra-Correlation (ICC) and Dice Similarity Coefficients (DSC) durchgeführt.

Die Analyse der Querschnitts- sowie der Longitudinalvolumina ergaben eine ausgeprägte Minderung im Cerebellum, Gehirnstamm und in der Pons (Fläche) sowie in supratentoriellen Strukturen bereits zur Geburt. Zum ersten Mal wurde ein globaler Volumenzuwachs im Kindesalter bei PCH2A nachgewiesen. Der Frontallappen war nicht stärker beeinträchtigt als andere supratentorielle Strukturen. Es zeigte sich stetiges supratentorielles Wachstum in den ersten 5 Jahren mit darauffolgender Abflachung. In den ersten 5 Jahren wurde kein Volumenrückgang in irgendeiner Gehirnstruktur beobachtet. Die Validierung zeigte hohe Präzision und Reproduzierbarkeit mit hohen ICC und DSC Werten.

Die bereits bei Geburt ausgeprägt verminderten infratentoriellen Volumina werden als Folge einer pränatalen Neurodegeneration interpretiert, die zur pontocerebellären Hypoplasie führt. Die Volumenzunahme aller Gehirnstrukturen in den ersten Lebensjahren widerlegen die Annahme einer kontinuierlich, fortschreitenden Neurodegeneration, und unterstützen stattdessen eine sekundäre Folge der primären infratentoriellen Hypoplasie auf die supratentorielle Gehirnentwicklung mit Mikrozephalie. Des Weiteren wird diese These durch den zwar geringfügigen aber klinischen Fortschritt der Kinder in den ersten Jahren unterstützt. Hinweise für eine Volumenabnahme bei älteren Kindern mit PCH2A können im Sinne einer spät einsetzenden Atrophie interpretiert werden, die sich wahrscheinlich bei fast allen Kindern mit PCH entwickelt.

Diese Studie vermittelt einen Einblick in die Rolle des zugrundeliegenden Gendefekts, der über eine primäre, cerebelläre Störung zu sekundären, schweren Störungen der cerebellär-cerebralen Netzwerke führt, gefolgt von einer ggf. späten Neurodegeneration.

## 7. Appendix

**Table 7-1: Patient data summary.** Each line contains the information per one patient, made up of gender, MRI format (either digital DICOM or analogue MRI film) and age in years. Since brain areas were measured in different planes, the corresponding slice thickness in axial, coronal and sagittal is listed as well as the selected sequence for the resulting plane.

Patient #	Gender	MRI format	Age in years	Slice thickness			Selected sequence		
				Axial [mm]	Coronal [mm]	Sagittal [mm]	Axial	Coronal	sagittal
1	female	DICOM	.88	5.5	6.0	5.5	T1	IR	T1
2	female	MRI film	3.17	6.6	.	3.3	IR	.	T2
3	male	MRI film	5.50	6.5	4.5	.	T1	T2	.
4	male	DICOM	17.06	7.2	5.5	5.5	T1	T1	T1
5	female	DICOM	1.97	6.5	6.5	1.0	T1	FLAIR	T1_3d
6	male	DICOM	.73	5.5	1.0	1.0	T2	T1_3d	T1_3d
7	male	MRI film	1.30	5.5	.	.	IR	.	.
8	female	DICOM	.19	6.0	6.0	4.0	IR	T1	T1
9	male	DICOM	3.21	6.6	3.6	.	T1	T2	.
10	female	MRI film	1.65	5.0	3.0	.	T1	T1	.
11	female	DICOM	.02	.9	.9	1.0	T1_3d	T1_3d	T1_3d
12	male	DICOM	1.08	4.4	5.5	4.8	IR	T2	T1
13	male	MRI film	7.43	6.0	.	.	IR	.	.
14	male	MRI film	.15	.	5.0	.	.	T2	.
15	female	DICOM	10.50	5.5	1.0	1.0	FLAIR	T1_3d	T1_3d

16	male	DICOM	.42	5.6	3.9	3.9	IR	T2	T1
17	male	DICOM	.44	4.0	3.6	3.3	T1	T2	T1
18	female	DICOM	.45	6.0	4.8	4.4	T1	FLAIR	T2
19	female	MRI film	.03	5.0	.	4.0	T1	.	T1
20	female	MRI film	.02	5.0	3.0	3.0	T1	T2	T2
21	female	DICOM	.16	5.0	3.3	3.0	T2	T2	T2
22	female	DICOM	.24	6.6	7.8	6.6	T2	T1	T2
23	female	DICOM	.38	.5	.5	1.3	T1_3d	T1_3d	T1_3d
24	male	MRI film	.90	.	6.0	.	.	T1	.

**Table 7-2 Control data summary.** Each line contains the information per one control made up of gender, and age in years [MRI format missing since all DICOM]. Since brain areas were measured in different planes, the corresponding slice thickness in axial, coronal and sagittal is listed as well as the selected sequence for the resulting plane.

Control #	Gender	Age in years	Slice thickness			Selected sequence		
			Axial [mm]	Coronal [mm]	Sagittal [mm]	axial plane	coronal plane	sagittal plane
1	male	16.08	1.0	1.0	1.0	T1_3d	T1_3d	T1_3d
2	male	5.50	1.3	.9	.9	T1_3d	T1_3d	T1_3d
3	male	6.58	1.0	1.0	1.0	T1_3d	T1_3d	T1_3d
4	female	2.04	1.0	1.0	3.0	T1_3d	T1_3d	T1_3d
5	female	.46	1.0	1.0	3.0	T1_3d	T1_3d	T1_3d
6	male	1.06	1.0	1.0	3.0	T1_3d	T1_3d	T1_3d
7	female	.04	1.0	1.0	3.0	T1_3d	T1_3d	T1_3d
8	female	.04	1.0	1.0	3.0	T1_3d	T1_3d	T1_3d
9	female	.80	1.0	1.0	3.0	T1_3d	T1_3d	T1_3d
10	male	1.03	1.0	1.0	3.0	T1_3d	T1_3d	T1_3d
11	female	3.17	1.0	1.0	3.0	T1_3d	T1_3d	T1_3d
12	male	.53	1.0	1.0	3.0	T1_3d	T1_3d	T1_3d
13	female	.20	1.0	1.0	3.0	T1_3d	T1_3d	T1_3d

14	female	.02	1.0	1.0	3.0	T1_3d	T1_3d	T1_3d
15	male	3.17	1.0	1.0	3.0	T1_3d	T1_3d	T1_3d
16	male	.06	1.0	1.0	3.0	T1_3d	T1_3d	T1_3d
17	female	.23	1.0	1.0	3.0	T1_3d	T1_3d	T1_3d
18	male	1.01	1.0	1.0	3.0	T1_3d	T1_3d	T1_3d
19	male	.31	1.0	1.0	3.0	T1_3d	T1_3d	T1_3d
20	female	1.64	1.0	1.0	3.0	T1_3d	T1_3d	T1_3d
21	female	.25	1.0	1.0	3.0	T1_3d	T1_3d	T1_3d
22	female	.55	1.0	1.0	3.0	T1_3d	T1_3d	T1_3d
23	male	.78	1.0	1.0	3.0	T1_3d	T1_3d	T1_3d
24	female	10.05	1.0	1.0	3.0	T1_3d	T1_3d	T1_3d

**Table 7-3: Longitudinal patient data summary.** Five patients ordered by age at time of scan. Scan numbers are arranged chronologically starting at earliest scan. Latest date of scan had been included in cross-sectional volume analysis, previous scans had to be excluded for main volumetric analysis. Since brain areas were measured in different planes, the corresponding slice thickness in axial, coronal and sagittal is listed as well as the selected sequence for the resulting plane.

Patient #	Scan #	Gender	MRI format	Age in years	Slice thickness			Selected Sequence		
					Axial [mm]	Coronal [mm]	Sagittal [mm]	axial plane	coronal plane	sagittal plane
pat_1	1	male	MRI film	.19	.	6.0	.	.	T1	.
	2			5.50	6.5	4.5	.	T1	T2	.
pat_2	1	female	DICOM	.04	5.2	5.6	3.3	FLAIR	T1	T1
	2			.28	5.2	6.0	.	T1	T1	.
	3			1.58	1.0	1.0	1.0	T1_3d	T1_3d	T1_3d
	4			1.97	6.5	6.5	1.0	T1	FLAIR	T1_3d
pat_3	1	male	MRI film	.21	4.9	.	3.8	IR	.	T2
	2			1.30	5.5	.	.	IR	.	.
pat_4	1	male	DICOM	.02	7.2	4.4	.	T1	T1	.
	2			.35	6.0	4.4	6.0	T1	T2	T1

	3			1.08	4.4	5.5	4.8	IR	T2	T1
pat_5	1	female	DICOM	.54	5.5	6.5	3.3	T1	IR	T2
	2			11.38	5.5	1.0	1.0	FLAIR	T1_3d	T1_3d

**Table 7-4 Patient volumetric results.** *The volumetric results of measured brain areas (cerebellum, brain stem, supratentorial brain and frontal lobe volume in ml. Note: For pons the area (mm<sup>2</sup>) was taken.) Also showing gender and age in years at MRI.*

Patient #	Gender	Age in years	Cerebellum [ml]	Brain stem [ml]	Supratentorial Brain [ml]	Frontal lobe [ml]	Pons [mm2]
1	female	.88	3.37	3.85	368.71	122.23	85.53
2	female	3.17	.	6.63	594.33	221.59	141.72
3	male	5.50	12.97	.	547.76	195.42	133.45
4	male	17.06	21.69	9.60	578.60	151.53	211.09
5	female	1.97	23.39	8.66	576.85	188.87	184.19
6	male	.73	13.82	5.66	590.35	188.66	215.57
7	male	1.30	.	.	485.73	163.68	118.83
8	female	.19	7.16	4.39	415.29	141.70	119.33
9	male	3.21	21.69	.	794.44	233.67	183.89
10	female	1.65	6.52	.	475.44	194.46	146.18
11	female	.02	5.19	3.31	285.20	87.37	121.29
12	male	1.08	12.23	5.41	533.75	171.07	117.19
13	male	7.43	.	.	575.22	195.01	156.30
14	male	.15	4.37	.	.	.	.
15	female	10.50	7.84	5.44	363.30	108.10	122.00
16	male	.42	9.96	5.39	481.33	152.10	136.72
17	male	.44	8.82	5.60	459.82	149.40	118.71
18	female	.45	10.87	4.57	505.30	193.39	134.03
19	female	.03	.	3.63	240.22	.	.
20	female	.02	4.51	2.98	284.30	94.16	161.42
21	female	.16	7.09	4.05	380.51	124.32	119.11
22	female	.24	7.54	5.32	430.12	158.57	110.78
23	female	.38	11.75	4.73	416.06	142.17	128.16
24	male	.90	12.54	.	.	.	.

**Table 7-5 Control volumetric results.** *The volumetric results of measured brain areas (cerebellum, brain stem, supratentorial brain and frontal lobe volume in ml. Note: For pons the area (mm<sup>2</sup>) was taken.) Also showing gender and age in years at MRI.*

Control #	Gender	Age in years	Cerebellum [ml]	Brain stem [ml]	Supratentorial Brain [ml]	Frontal lobe [ml]	Pons [mm <sup>2</sup> ]
1	male	16.08	159.19	24.13	1095.98	376.53	615.00
2	male	5.50	126.44	21.40	1206.26	419.57	549.66
3	male	6.58	138.95	24.07	1330.98	476.93	619.00
4	female	2.04	115.31	15.86	807.41	266.15	511.00
5	female	.46	59.38	12.93	524.22	177.94	318.53
6	male	1.06	114.21	16.10	906.79	282.11	499.73
7	female	.04	32.89	7.81	436.10	151.96	235.56
8	female	.04	30.89	8.29	424.62	132.38	255.58
9	female	.80	103.20	15.12	820.87	251.94	373.00
10	male	1.03	117.47	17.80	858.91	293.37	440.00
11	female	3.17	131.74	21.28	917.42	319.05	629.00
12	male	.53	84.44	13.52	699.22	226.48	434.87
13	female	.20	47.52	9.54	484.12	146.93	322.00
14	female	.02	27.06	7.68	381.37	133.03	241.00
15	male	3.17	153.91	23.19	1154.36	388.59	641.00
16	male	.06	35.81	9.50	457.58	157.66	264.00
17	female	.23	51.42	10.43	486.75	158.99	347.00
18	male	1.01	119.60	14.47	1021.88	345.96	403.40
19	male	.31	54.37	10.77	574.29	204.98	351.91
20	female	1.64	93.18	14.57	830.86	270.20	451.58
21	female	.25	53.50	10.37	510.62	165.53	331.00
22	female	.55	77.31	12.17	621.26	183.27	326.00
23	male	.78	103.23	16.29	770.75	248.95	471.11
24	female	10.05	154.70	23.46	1016.72	324.24	642.00

**Table 7-6 Longitudinal volumetric results in five PCH2A patients.** *Volumetric results ordered according to patient and chronologically at time of MRI for patients with more than one scan. The volumetric results of measured brain areas (cerebellum, brain stem, supratentorial brain and frontal lobe volume in ml. Note: For pons the area (mm<sup>2</sup>) was taken.)*

	Gender	Scan #	Age in years at MRI	Cerebellum [ml]	Brain stem [ml]	Supratentorial Brain [ml]	Frontal lobe [ml]	Pons [mm <sup>2</sup> ]
pat_1	male	1	.19	4.78	.	.	.	.



		2	5.50	12.97	.	547.76	195.42	133.45
pat_2	female	1	.04	8.25	3.87	301.59	88.12	139.47
		2	.28	13.16	.	420.41	120.35	133.59
		3	1.58	25.38	8.47	596.00	172.56	175.35
		4	1.97	23.39	8.66	576.85	188.87	184.19
pat_3	male	1	.21	.	3.87	372.20	151.04	101.93
		2	1.30	.	.	485.73	163.68	118.83
pat_4	male	1	.02	5.13	.	271.80	91.97	105.44
		2	.35	7.84	5.79	436.75	154.25	126.82
		3	1.08	12.23	5.41	533.75	171.07	117.19
pat_5	female	1	.54	7.97	4.54	387.56	116.61	134.89
		2	10.50	7.84	5.44	363.30	108.10	122.00

**Table 7-7 Validation results in 5 patients and 5 controls.** Supratentorial [ml] and cerebellar [ml] volumes were re-measured in the digital to analogue approach (Voxel to pixel), KE to KE (intra-rater testing) and SG to KE (inter-rater testing). Additionally, DSC (Dice correlation coefficient) for spatial overlap for intra-rater and inter-rater testing in supratentorial and cerebellar samples were calculated. Validation ID: val\_c\_# referring to controls and val\_p\_# to patients.

validation ID	Supratentorial measurements					Cerebellar measurements				
	Supratentorial brain volume [ml] for			DSC for supratentorial		Cerebellar volume [ml] for			DSC for cerebellar	
	Voxel to pixel	intra-rater test	inter-rater test	intra-rater test	inter-rater test	Voxel to pixel	intra-rater test	inter-rater test	intra-rater test	inter-rater test
val_c_1	575.37	603.04	599.88	.98	.98	60.38	56.20	58.60	.91	.95
val_c_2	947.91	916.71	918.41	1.00	.99	124.89	125.60	124.50	.96	.98
val_c_3	634.91	652.05	657.20	.96	.98	61.59	67.30	67.70	.92	.95
val_c_4	433.83	449.09	449.14	.98	.98	34.57	33.50	32.70	.92	.95
val_c_5	1037.60	1030.77	1033.39	.98	.99	125.19	122.10	118.50	.92	.96
val_p_6	307.46	297.53	298.84	.98	.99	7.70	7.70	7.70	.91	.96
val_p_7	431.32	425.71	422.39	.94	.96	7.75	7.00	6.70	.74	.86
val_p_8	801.05	799.41	800.20	.99	.99	19.44	18.50	19.10	.89	.95
val_p_9	546.58	526.90	532.14	.95	.98	12.33	12.50	13.40	.90	.93
val_p_10	379.55	378.88	370.28	.96	.97	5.49	7.60	7.80	.90	.94

## 8. Bibliography

- Aboulezz, A.O., Sartor, K., Geyer, C.A., Gado, M.H., 1985. Position of cerebellar tonsils in the normal population and in patients with Chiari malformation: a quantitative approach with MR imaging. *J. Comput. Assist. Tomogr.* 9, 1033–1036.
- Anderson, C., Davies, J.H., Lamont, L., Foulds, N., 2011. Early pontocerebellar hypoplasia with vanishing testes: A new syndrome? *Am. J. Med. Genet. A.* 155A, 667–672. <https://doi.org/10.1002/ajmg.a.33897>
- Barth, P.G., 1993. Pontocerebellar hypoplasias. An overview of a group of inherited neurodegenerative disorders with fetal onset. *Brain Dev.* 15, 411–422.
- Barth, P.G., Aronica, E., de Vries, L., Nikkels, P.G.J., Scheper, W., Hoozemans, J.J., Poll-The, B.-T., Troost, D., 2007. Pontocerebellar hypoplasia type 2: a neuropathological update. *Acta Neuropathol. (Berl.)* 114, 373–386. <https://doi.org/10.1007/s00401-007-0263-0>
- Barth, P.G., Blennow, G., Lenard, H.G., Begeer, J.H., van der Kley, J.M., Hanefeld, F., Peters, A.C., Valk, J., 1995. The syndrome of autosomal recessive pontocerebellar hypoplasia, microcephaly, and extrapyramidal dyskinesia (pontocerebellar hypoplasia type 2): compiled data from 10 pedigrees. *Neurology* 45, 311–317.
- Barth, P.G., Ryan, M.M., Webster, R.I., Aronica, E., Kan, A., Ramkema, M., Jardine, P., Poll-The, B.T., 2008. Rhabdomyolysis in pontocerebellar hypoplasia type 2 (PCH-2). *Neuromuscul. Disord. NMD* 18, 52–58. <https://doi.org/10.1016/j.nmd.2007.08.001>
- Barth, P.G., Vrensen, G.F., Uylings, H.B., Oorthuys, J.W., Stam, F.C., 1990. Inherited syndrome of microcephaly, dyskinesia and pontocerebellar hypoplasia: a systemic atrophy with early onset. *J. Neurol. Sci.* 97, 25–42.
- Biemond, A., 1955. Hypoplasia ponto-neocerebellaris, with malformation of the dentate nucleus. *Folia Psychiatr. Neurol. Neurochir. Neerlandica* 58, 2–7.
- Bland, J.M., Altman, D.G., 1990. A note on the use of the intraclass correlation coefficient in the evaluation of agreement between two methods of measurement. *Comput. Biol. Med.* 20, 337–340.
- Brain Development Cooperative Group, 2012. Total and regional brain volumes in a population-based normative sample from 4 to 18 years: the NIH MRI Study of Normal Brain Development. *Cereb. Cortex N. Y. N* 1991 22, 1–12. <https://doi.org/10.1093/cercor/bhr018>
- Brun, R., 1917. Zur Kenntnis der Bildungsfehler des Kleinhirns. Epikritische Bemerkungen zur Entwicklungspathologie, Morphologie und Klinik der umschriebenen Entwicklungshemmungen des Neocerebellums. *Schweiz Arch Neurol Psychiatr* 48–105.

- Budde, B.S., Namavar, Y., Barth, P.G., Poll-The, B.T., Nürnberg, G., Becker, C., van Ruissen, F., Weterman, M.A.J., Fluiter, K., te Beek, E.T., Aronica, E., van der Knaap, M.S., Höhne, W., Toliat, M.R., Crow, Y.J., Steinling, M., Voit, T., Roelenso, F., Brussel, W., Brockmann, K., Kyllerman, M., Boltshauser, E., Hammersen, G., Willemsen, M., Basel-Vanagaite, L., Krägeloh-Mann, I., de Vries, L.S., Sztriha, L., Muntoni, F., Ferrie, C.D., Battini, R., Hennekam, R.C.M., Grillo, E., Beemer, F.A., Stoets, L.M.E., Wollnik, B., Nürnberg, P., Baas, F., 2008. tRNA splicing endonuclease mutations cause pontocerebellar hypoplasia. *Nat. Genet.* 40, 1113–1118. <https://doi.org/10.1038/ng.204>
- Collier, D.C., Burnett, S.S., Amin, M., Bilton, S., Brooks, C., Ryan, A., Roniger, D., Tran, D., Starkschall, G., 2003. Assessment of consistency in contouring of normal-tissue anatomic structures. *J. Appl. Clin. Med. Phys. Am. Coll. Med. Phys.* 4, 17–24.
- Dennis, E.L., Thompson, P.M., 2013. Typical and atypical brain development: a review of neuroimaging studies. *Dialogues Clin. Neurosci.* 15, 359–384.
- Despotović, I., Goossens, B., Philips, W., 2015. MRI segmentation of the human brain: challenges, methods, and applications. *Comput. Math. Methods Med.* 2015, 450341. <https://doi.org/10.1155/2015/450341>
- Ekert, K., Groeschel, S., Sánchez-Albisua, I., Frölich, S., Dieckmann, A., Engel, C., Krägeloh-Mann, I., 2016. Brain morphometry in Pontocerebellar Hypoplasia type 2. *Orphanet J. Rare Dis.* 11, 100. <https://doi.org/10.1186/s13023-016-0481-4>
- Evans, A.C., Brain Development Cooperative Group, 2006. The NIH MRI study of normal brain development. *NeuroImage* 30, 184–202. <https://doi.org/10.1016/j.neuroimage.2005.09.068>
- Gadisseux, J.F., Rodriguez, J., Lyon, G., 1984. Pontoneocerebellar hypoplasia--a probable consequence of prenatal destruction of the pontine nuclei and a possible role of phenytoin intoxication. *Clin. Neuropathol.* 3, 160–167.
- Goasdoué, P., Rodriguez, D., Moutard, M.L., Robain, O., Lalande, G., Adamsbaum, C., 2001. Pontoneocerebellar hypoplasia: definition of MR features. *Pediatr. Radiol.* 31, 613–618. <https://doi.org/10.1007/s0024710310613>
- Goutières, F., Aicardi, J., Farkas, E., 1977. Anterior horn cell disease associated with pontocerebellar hypoplasia in infants. *J. Neurol. Neurosurg. Psychiatry* 40, 370–378.
- Graham, J.M., Spencer, A.H., Grinberg, I., Niesen, C.E., Platt, L.D., Maya, M., Namavar, Y., Baas, F., Dobyns, W.B., 2010. Molecular and neuroimaging findings in pontocerebellar hypoplasia type 2 (PCH2): is prenatal diagnosis possible? *Am. J. Med. Genet. A.* 152A, 2268–2276. <https://doi.org/10.1002/ajmg.a.33579>
- Groeschel, S., Vollmer, B., King, M.D., Connelly, A., 2010. Developmental changes in cerebral grey and white matter volume from infancy to adulthood. *Int. J. Dev.*

Neurosci. Off. J. Int. Soc. Dev. Neurosci. 28, 481–489.  
<https://doi.org/10.1016/j.ijdevneu.2010.06.004>

- Guibaud, L., 2004. Practical approach to prenatal posterior fossa abnormalities using MRI. *Pediatr. Radiol.* 34, 700–711. <https://doi.org/10.1007/s00247-004-1248-y>
- Johnsen, S.D., Bodensteiner, J.B., Lotze, T.E., 2005. Frequency and nature of cerebellar injury in the extremely premature survivor with cerebral palsy. *J. Child Neurol.* 20, 60–64.
- Lerch, J.P., van der Kouwe, A.J.W., Raznahan, A., Paus, T., Johansen-Berg, H., Miller, K.L., Smith, S.M., Fischl, B., Sotiropoulos, S.N., 2017. Studying neuroanatomy using MRI. *Nat. Neurosci.* 20, 314–326. <https://doi.org/10.1038/nn.4501>
- Limperopoulos, C., Bassan, H., Gauvreau, K., Robertson, R.L., Sullivan, N.R., Benson, C.B., Avery, L., Stewart, J., Md, J.S.S., Ringer, S.A., Volpe, J.J., duPlessis, A.J., 2007. Does Cerebellar Injury in Premature Infants Contribute to the High Prevalence of Long-term Cognitive, Learning, and Behavioral Disability in Survivors? *Pediatrics* 120, 584–593. <https://doi.org/10.1542/peds.2007-1041>
- Makropoulos, A., Aljabar, P., Wright, R., Hüning, B., Merchant, N., Arichi, T., Tusor, N., Hajnal, J.V., Edwards, A.D., Counsell, S.J., Rueckert, D., 2016. Regional growth and atlas of the developing human brain. *NeuroImage* 125, 456–478. <https://doi.org/10.1016/j.neuroimage.2015.10.047>
- Messerschmidt, A., Brugger, P.C., Boltshauser, E., Zoder, G., Sterniste, W., Birnbacher, R., Prayer, D., 2005. Disruption of Cerebellar Development: Potential Complication of Extreme Prematurity. *Am. J. Neuroradiol.* 26, 1659–1667.
- Middleton, F.A., Strick, P.L., 1998. The cerebellum: an overview. *Trends Cogn. Sci.* 2, 305–306. [https://doi.org/10.1016/S1364-6613\(98\)01224-8](https://doi.org/10.1016/S1364-6613(98)01224-8)
- Namavar, Y., Barth, P.G., Kasher, P.R., van Ruissen, F., Brockmann, K., Bernert, G., Writzl, K., Ventura, K., Cheng, E.Y., Ferriero, D.M., Basel-Vanagaite, L., Eggens, V.R.C., Krägeloh-Mann, I., De Meirleir, L., King, M., Graham, J.M., Jr, von Moers, A., Knoers, N., Sztriha, L., Korinthenberg, R., Dobyns, W.B., Baas, F., Poll-The, B.T., 2011a. Clinical, neuroradiological and genetic findings in pontocerebellar hypoplasia. *Brain J. Neurol.* 134, 143–156. <https://doi.org/10.1093/brain/awq287>
- Namavar, Y., Barth, P.G., Poll-The, B.T., Baas, F., 2011b. Classification, diagnosis and potential mechanisms in Pontocerebellar Hypoplasia. *Orphanet J. Rare Dis.* 6, 50. <https://doi.org/10.1186/1750-1172-6-50>
- Namavar, Y., Eggens, V.R., Barth, P.G., Baas, F., 2016. TSEN54-Related Pontocerebellar Hypoplasia, in: Pagon, R.A., Adam, M.P., Ardinger, H.H., Wallace, S.E., Amemiya, A., Bean, L.J., Bird, T.D., Ledbetter, N., Mefford, H.C., Smith, R.J., Stephens, K. (Eds.), *GeneReviews*(®). University of Washington, Seattle, Seattle (WA).

- Ramnani, N., 2006. The primate cortico-cerebellar system: anatomy and function. *Nat. Rev. Neurosci.* 7, 511–522. <https://doi.org/10.1038/nrn1953>
- Rasband, Wayne, 2016. ImageJ Listed Features [WWW Document]. URL <https://imagej.nih.gov/ij/features.html> (accessed 4.17.16).
- Sánchez-Albisua, I., Frölich, S., Barth, P.G., Steinlin, M., Krägeloh-Mann, I., 2014. Natural course of pontocerebellar hypoplasia type 2A. *Orphanet J. Rare Dis.* 9, 70. <https://doi.org/10.1186/1750-1172-9-70>
- Schneider, C.A., Rasband, W.S., Eliceiri, K.W., 2012. NIH Image to ImageJ: 25 years of image analysis. *Nat. Methods* 9, 671–675. <https://doi.org/10.1038/nmeth.2089>
- Shrout, P.E., Fleiss, J.L., 1979. Intraclass correlations: uses in assessing rater reliability. *Psychol. Bull.* 86, 420–428.
- Squier, W., Hope, P.L., Lindenbaum, R.H., 1990. Neocerebellar hypoplasia in a neonate following intra-uterine exposure to anticonvulsants. *Dev. Med. Child Neurol.* 32, 737–742.
- Steinlin, M., Klein, A., Haas-Lude, K., Zafeiriou, D., Strozzi, S., Müller, T., Gubser-Mercati, D., Schmitt Mechelke, T., Krägeloh-Mann, I., Boltshauser, E., 2007. Pontocerebellar hypoplasia type 2: variability in clinical and imaging findings. *Eur. J. Paediatr. Neurol. EJPN Off. J. Eur. Paediatr. Neurol. Soc.* 11, 146–152. <https://doi.org/10.1016/j.ejpn.2006.11.012>
- Stoodley, C.J., Schmahmann, J.D., 2009. Functional topography in the human cerebellum: A meta-analysis of neuroimaging studies. *NeuroImage* 44, 489–501. <https://doi.org/10.1016/j.neuroimage.2008.08.039>
- Tiemeier, H., Lenroot, R.K., Greenstein, D.K., Tran, L., Pierson, R., Giedd, J.N., 2010. Cerebellum development during childhood and adolescence: a longitudinal morphometric MRI study. *NeuroImage* 49, 63–70. <https://doi.org/10.1016/j.neuroimage.2009.08.016>
- Tocchio, S., Kline-Fath, B., Kanal, E., Schmithorst, V.J., Panigrahy, A., 2015. MRI Evaluation and Safety in the Developing Brain. *Semin. Perinatol.* 39, 73–104. <https://doi.org/10.1053/j.semperi.2015.01.002>
- Tournier, J.-D., Calamante, F., Connelly, A., 2012. MRtrix: Diffusion tractography in crossing fiber regions. *Int. J. Imaging Syst. Technol.* 22, 53–66. <https://doi.org/10.1002/ima.22005>
- Trepel, M., 2008. *Neuroanatomie: Struktur und Funktion*, 4. ed. Elsevier, Urban & Fischer, Munich.

- Uhl, M., Pawlik, H., Laubenberger, J., Darge, K., Baborie, A., Korinthenberg, R., Langer, M., 1998. MR findings in pontocerebellar hypoplasia. *Pediatr. Radiol.* 28, 547–551. <https://doi.org/10.1007/s002470050410>
- Yushkevich, P.A., Piven, J., Hazlett, H.C., Smith, R.G., Ho, S., Gee, J.C., Gerig, G., 2006. User-guided 3D active contour segmentation of anatomical structures: significantly improved efficiency and reliability. *NeuroImage* 31, 1116–1128. <https://doi.org/10.1016/j.neuroimage.2006.01.015>
- Yushkevich, Paul, 2016. ITK-SNAP Home Page Wiki [WWW Document]. URL <http://www.itksnap.org/pmwiki/pmwiki.php> (accessed 4.17.16).
- Zou, K.H., Warfield, S.K., Bharatha, A., Tempany, C.M.C., Kaus, M.R., Haker, S.J., Wells, W.M., Jolesz, F.A., Kikinis, R., 2004. Statistical Validation of Image Segmentation Quality Based on a Spatial Overlap Index. *Acad. Radiol.* 11, 178–189. [https://doi.org/10.1016/S1076-6332\(03\)00671-8](https://doi.org/10.1016/S1076-6332(03)00671-8)

## 9. Contributions

This study was carried out at the University Children's Hospital Tübingen under the supervision of professor Krägeloh-Mann. Samuel Gröschel, Kaspar Ekert, Iciar Sánchez-Albisua and Ingeborg Krägeloh-Mann conceived the study and drafted the manuscript. Collection of patient data was carried out by Saskia Frölich, doctoral candidate of previous PCH2A study (Sánchez-Albisua et al., 2014), Andrea Dieckmann and Iciar Sánchez.

The volumetric MRI analysis methods used here were carried out by Kaspar Ekert and the inter-rater validation process by Samuel Gröschel.

Statistical Assessment was carried out by Dr. Corinna Engel, Department of Child Neurology, resort biometrics, Children's Hospital at the University of Tübingen, Hoppe-Seyler-Str. 1, 72072 Tübingen, Germany.

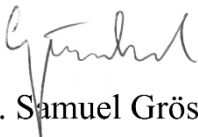
Samuel Gröschel and Ingeborg Krägeloh-Mann critically revised the doctoral thesis.

I assert that I composed the manuscript myself under guidance by Samuel Gröschel and that no further sources other than referenced have been used.


Dated Tübingen Thursday, 03 August 2017.



Kaspar Ekert



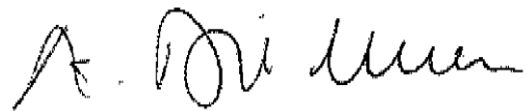
Dr. med. Samuel Gröschel



Dr. med. Iciar Sánchez-Albisua



Saskia Frölich



Dr. med. Andrea Dieckmann



Dr. Corinna Engel



Prof. Dr. med. Ingeborg Krägeloh-Mann



## 10. Publications

Ekert, K\*, Groeschel, S\*, Sánchez-Albisua, I., Frölich, S., Dieckmann, A., Engel, C., Krägeloh-Mann, I., 2016. Brain morphometry in Pontocerebellar Hypoplasia type 2. Orphanet J. Rare Dis. 11, 100. doi:10.1186/s13023-016-0481-4. \*equal contribution.

Groeschel, S., Ekert, K., Sánchez-Albisua, I., Frölich, S., Krägeloh-Mann, I., 2014. Brain Morphometry in Pontocerebellar Hypoplasia Type 2. Neuropediatrics 45. doi:10.1055/s-0034-1390551

## **11. Acknowledgements**

Für die sehr gute Leitung von Frau Prof. Krägeloh-Mann möchte ich mich herzlichst bedanken.

Besonders danken möchte ich Samuel Gröschel für die hervorragende Betreuung und die gute Zusammenarbeit während der Erarbeitung meiner Dissertation.

Ein besonderer Dank gilt insbesondere meinen Eltern, die mich stets auf meinem Weg durch das Studium unterstützt haben.